

Neutrons on a surface of liquid helium

P. D. Grigoriev*

L. D. Landau Institute for Theoretical Physics, Chernogolovka, Moscow region, 142432, Russia;

O. Zimmer† and T. Ziman

Institut Laue-Langevin, BP 156, 6 rue Jules Horowitz, 38042 Grenoble Cedex 9, France

A. D. Grigoriev

Samara State University, Samara, Russia

(Dated: March 5, 2022)

We investigate the possibility of ultracold neutron (UCN) storage in quantum states defined by the combined potentials of the Earth’s gravity and the neutron optical repulsion by a horizontal surface of liquid helium. We analyse the stability of the lowest quantum state, which is most susceptible to perturbations due to surface excitations, against scattering by helium atoms in the vapor and by excitations of the liquid, comprised of riplons, phonons and surfons. This is an unusual scattering problem since the kinetic energy of the neutron parallel to the surface may be much greater than the binding energies perpendicular. The total scattering time constant of these UCNs at 0.7 K is found to exceed one hour, and rapidly increasing with decreasing temperature. Such low scattering rates should enable high-precision measurements of the scheme of discrete energy levels, thus providing improved access to short-range gravity. The system might also be useful for neutron β -decay experiments. We also sketch new experimental concepts for level population and trapping of UCNs above a flat horizontal mirror.

I. INTRODUCTION

Slow neutrons play an important role in low-energy particle physics as a tool and an object, in investigations of the free neutron’s properties and its interactions with known or hypothetic fields with high precision [1–3]. A particular class of experiments employs neutrons with energy lower than the neutron optical potential of typical materials, i.e. in the order of up to 300 neV. These so-called ultracold neutrons (UCNs) can be imprisoned for many hundreds of seconds in well-designed “neutron bottles”. By virtue of the neutron magnetic moment of 60 neV/T magnetic trapping is feasible too, and also the gravitational interaction with a potential difference of 100 neV per meter rise can play its role in UCN storage and manipulation [4, 5]. Perhaps the most prominent application of UCNs is the search for a non-vanishing electric dipole moment of the neutron. Finding a finite value or just improving current limits is a way of investigating new mechanisms of CP violation beyond the standard model’s complex phase of the weak quark mixing CKM matrix, and the matter-antimatter asymmetry in the universe [7]. Latest experimental results were published in Refs. [8, 9]. Similarly long standing are the experimental efforts to determine the neutron lifetime with high accuracy. Its value enters the calculations of weak reaction rates in big-bang nucleosynthesis and stellar fusion [10, 11], and it is also crucial for deriving the weak axial-vector and vector coupling constants of the nucleon needed to calculate many

important semi-leptonic cross sections.

Discrete energy levels of UCNs in the Earth’s gravitational field were proposed by Lushikov and Frank in 1978 [12], and demonstrated experimentally in the past decade [13–15]. Precise measurements of the energy levels, that are not equi-distant, offer an interesting tool for tests of various new scenarios of particle physics. The range of effects investigated is determined by the characteristic size, several tens of micrometers, with which the neutron wave functions are bound in one dimension. Deviations from the Newton’s gravity law at small distances can for instance be interpreted as a signal of large extra dimensions at the sub-millimeter scale [16, 17] or as a hint for dark-energy “chameleon” fields [18, 19]. A recent development, called gravity resonance spectroscopy (GRS), where transitions between levels are induced by vibrating the mirror, has paved a way towards sensitive tests of such scenarios [20] (note, however, a strong competition from atomic physics in the chameleon search [21]). A competing, alternative, method will employ oscillating magnetic field gradients [22, 23]. The GRS experiment described in Ref. [19] has already set stringent limits on chameleons. It has also constrained axion-like particles, improving the result of an analysis of the non-resonant gravity experiment described in Ref. [24]. A method not relying on spatial quantum states of the neutron employs spin precession of trapped UCNs close to a heavy mirror [25]. The sensitivity of the GRS experiment was almost as good as a first search of that latter type [26] and recently much improved [27], still with potential for large further gains in sensitivity. For the gravity experiment too, a large gain is still to be expected, notably once an adaptation of Ramsey’s molecular beam technique of separated oscillatory fields to GRS is implemented [28]. In addition, a search for a

*Electronic address: grigorev@itp.ac.ru

†Electronic address: zimmer@ill.fr

non-zero neutron charge based on the latter technique has been proposed [29].

All current experiments on gravitational quantum states of the neutron employ highly polished quartz mirrors. These are expensive, limited to sizes of several tens of centimeters, and they have to be horizontally levelled by some active means. In this respect, using a liquid surface as a mirror might initiate a qualitatively new approach. On one hand it may furnish a remedy to the aforementioned limitations. On the other hand, the interactions of neutrons prepared in gravity states with excitations or structural decorations of the liquid surface could enlarge the applications of these states to investigations of the surface physics. The present article provides a theoretical investigation of the possibility to store UCNs in the lowest gravitational energy states on the liquid helium surface, by analysis of scattering by helium atoms in the gas phase and by various excitations in both the bulk and at the surface of the liquid helium. Obviously, a long storage time constant is a necessary condition for conducting experiments using a mirror made of this quantum liquid. A separate section sketches some experimental concepts addressing issues arising in real studies employing those neutrons, notably population, trapping and detection.

Properties of neutrons on the liquid helium surface are, in several aspects, similar to those of electrons. The two-dimensional electron gas on a surface of dielectric media has for many decades been a wide subject of research (for reviews see, e.g., [30–32]). In contrast to the gravitational force in the neutron case, the electrons are attracted to the boundary by the electric image forces through which they become localized in the direction perpendicular to the surface. The surface of superfluid helium has no solid defects (like impurities, dislocations, etc.) and offers a unique opportunity to create an extremely pure 2D electron gas. The mobility of electrons in this gas usually exceeds more than thousand times that of electrons in 2D quantum wells in heterostructures. The system thus simulates a solid-state 2D quantum well without disorder. Many fundamental properties of a 2D electron gas have been studied with the help of electrons on the surfaces of liquid helium. Various electronic quantum objects can be experimentally realized on the liquid helium surface, such as quantum dots [33], 1D electron wires [34], quantum rings [35], and others. The electrons on the liquid helium surface may also serve for an experimental realization of a set of quantum bits with very long decoherence time [36]. If neutrons can be made to rest in surface states in sufficient densities we can hope for comparable studies using neutrons rather than electrons, and possible new states of quantum matter.

II. NEUTRONS ABOVE A FLAT HELIUM SURFACE

We consider a plane boundary between superfluid ${}^4\text{He}$ (situated at vertical coordinate $z < 0$) and its saturated

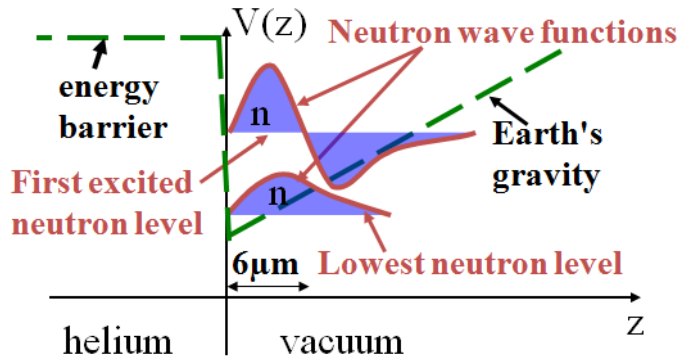


FIG. 1: Schematic representation of the vertical potential and the first two states of a neutron above a horizontal mirror of liquid helium.

vapor ($z > 0$). The interaction of a neutron with a ${}^4\text{He}$ atom with nuclear coordinate \mathbf{R}_i can be expressed as a Fermi pseudo-potential given by

$$V_i(\mathbf{r}) = U\delta^{(3)}(\mathbf{r} - \mathbf{R}_i) \equiv \frac{2\pi\hbar^2 a_{\text{He}}}{m}\delta^{(3)}(\mathbf{r} - \mathbf{R}_i), \quad (1)$$

where $\delta^{(3)}(\mathbf{r})$ is the 3D Dirac delta function. Substituting the bound coherent neutron scattering length $a_{\text{He}} = 3.26 \times 10^{-13}$ cm of a ${}^4\text{He}$ atom and the neutron mass $m = 1.675 \times 10^{-24}$ g, one obtains the value $U = 1.36 \times 10^{-42}$ erg cm^3 [1 erg = 10^{-7} J $\approx 6.25 \times 10^{11}$ eV]. Within the helium bulk the neutron interacts with a "forest" of δ -function potentials with volume concentration given by the particle density of ${}^4\text{He}$ atoms, $n_{\text{He}} \approx 21.8 \text{ nm}^{-3}$ at $T < 2.18$ K. As a result of the interference of a plane incident wave with the spherical scattered waves from each ${}^4\text{He}$ nucleus, neutron propagation in the bulk can be described by a constant neutron optical potential given by the spatially averaged pseudo-potentials of the helium atoms in a volume Ω containing many atoms, i.e.

$$\begin{aligned} V_0 &= \Omega^{-1} \int_{\Omega} \sum_i V_i(\mathbf{r}) d^3\mathbf{r} = Un_{\text{He}} \\ &\approx 2.965 \times 10^{-20} \text{ erg} = 18.5 \text{ neV}. \end{aligned} \quad (2)$$

Above the ${}^4\text{He}$ surface, neglecting interactions with the helium vapor discussed further below, the neutron is exposed to the gravity potential,

$$V(z) = mgz, \quad (3)$$

where $g = 981 \text{ cm/s}^2$ is the acceleration of free fall (gravitational acceleration at Earth's surface), giving the gravity force for the neutron, $mg = 1.643 \times 10^{-21}$ erg/cm = 1.026 neV/cm.

One can easily solve the one-dimensional Schrödinger equation for a neutron in the potential given by Eqs. (2) and (3) and shown in Fig. 1. The corresponding Hamiltonian is given by

$$\hat{H}_0 = -\frac{\hbar^2 \hat{\Delta}}{2m} + mgz + V_0\theta(-z), \quad (4)$$

where $\hat{\Delta} = \nabla^2$ is the Laplace operator, ∇ is the gradient operator, and $\theta(x)$ is the step function [$\theta(x) = 1$ for $x > 0$ and $\theta(x) = 0$ for $x \leq 0$]. The x , y and z coordinates separate in this equation, and the neutron wave function is given by a product

$$\psi(\mathbf{r}) = \psi_{\parallel}(\mathbf{r}_{\parallel}) \psi_{\perp}(z), \quad (5)$$

where $\mathbf{r}_{\parallel} = (x, y)$ is the 2D coordinate vector along the surface, while $\mathbf{r} = (x, y, z)$ stands for the 3D coordinate vector. In the x - y plane, the neutron wave function is given by a normalized plane wave,

$$\psi_{\parallel}(\mathbf{r}_{\parallel}) = S^{-1/2} \exp(i\mathbf{p}_{\parallel}\mathbf{r}_{\parallel}/\hbar), \quad (6)$$

where S is the He surface area, and \mathbf{p}_{\parallel} is the 2D neutron momentum along the surface. For $z < 0$ we can neglect the weak gravitational potential given by Eq. (3) as compared to the much stronger potential wall given by Eq. (2). The z -dependent part of the neutron wave function in this region is then approximately given by

$$\psi_{\perp}(z) = \psi_{\perp}(0) \exp(\kappa z) \quad (z < 0, E_{\perp} < V_0), \quad (7)$$

where $\kappa = ik_{\perp} = \sqrt{2m(V_0 - E_{\perp})}/\hbar$, and E_{\perp} is the neutron kinetic energy along the z -axis. For $E_{\perp} \ll V_0$, $\kappa_0 \equiv \sqrt{2mV_0}/\hbar \approx 2.4 \times 10^5 \text{ cm}^{-1}$, i.e. the neutron penetration depth into the liquid helium is

$$\kappa_0^{-1} \approx 33 \text{ nm}. \quad (8)$$

For $z > 0$, the neutron wave function is given by

$$\psi_{\perp}(z) = C \text{Ai}[(z - E_{\perp}/mg)/z_0] \quad (z > 0), \quad (9)$$

where C is a normalization coefficient, $\text{Ai}(x)$ is the Airy function, and

$$z_0 \equiv (\hbar^2/2m^2g)^{1/3} = 5.87 \text{ } \mu\text{m} \quad (10)$$

is a characteristic length scale of the neutron wave function in low energy states. For $z > E_{\perp}/mg$ the wave function given in Eq. (9) decreases exponentially. For $E_{\perp} < V_0$ the energy spectrum of the z -axis motion of a neutron above the liquid-helium surface is quantized. The eigenvalues of energy are given by the boundary condition at $z = 0$, i.e.

$$\frac{\psi'_{\perp}(0)}{\psi_{\perp}(0)} = \kappa = \frac{\sqrt{2m(V_0 - E_{\perp})}}{\hbar} = \frac{\text{Ai}'(-u)}{z_0 \text{Ai}(-u)}, \quad (11)$$

where the prime indicates the derivative, and

$$u \equiv E_{\perp}/mgz_0. \quad (12)$$

Equation (11) for finite V_0 can be solved only numerically. A characteristic scale of separations between lowest energy levels is given by $mgz_0 = (\hbar^2 mg^2/2)^{1/3} = 0.96 \times 10^{-24} \text{ erg} = 0.6 \text{ peV}$.

In the limit $V_0 \rightarrow \infty$ the energy levels are given by

$$E_n = mgz_0 \alpha_{n+1}, \quad n = 0, 1, \dots, \quad (13)$$

where $-\alpha_{n+1}$ are the zeros of the Airy function,

$$\alpha_1 = 2.338, \quad \alpha_2 = 4.088, \quad \alpha_3 = 5.521, \quad \alpha_4 = 6.787. \quad (14)$$

For $n \gg 1$,

$$\alpha_n \approx (3\pi n/2)^{2/3} - (\pi^2/96n)^{1/3}. \quad (15)$$

Note that this expression provides a highly accurate approximation even for small n : for α_1 the error is only $|\Delta\alpha/\alpha| \approx 0.0018$, and further decreases for $n > 1$, e.g., $|\Delta\alpha/\alpha| \approx 0.0005$ for α_2 .

For finite V_0 , Eq. (11) can be rewritten as

$$\text{Ai}'(-u) = \text{Ai}(-u) \sqrt{\eta_0 - u}, \quad (16)$$

using the dimensionless constant

$$\eta_0 \equiv V_0/mgz_0 = 3.078 \times 10^4, \quad (17)$$

evaluated on the r.h.s. for V_0 of superfluid He. Eqs. (16) and (17) give the following values of $\alpha_{n+1}^{\text{He}} = E_n/mgz_0$ of the discrete energy of a neutron above the He mirror:

$$\alpha_1^{\text{He}} = 2.332, \quad \alpha_2^{\text{He}} = 4.082, \quad \alpha_3^{\text{He}} = 5.515, \quad \alpha_4^{\text{He}} = 6.781. \quad (18)$$

These values are indeed very close to the values α_n for $V_0 \rightarrow \infty$ [compare Eq. (14)], because $\eta_0 \gg 1$. The neutron wave functions above liquid He are also very close to those for $V_0 \rightarrow \infty$, except for a region close to $z = 0$, where they acquire values $\psi_{\perp n}(0) = C_n \text{Ai}(-\alpha_{n+1}^{\text{He}})$ which are small but finite, since $\alpha_{n+1}^{\text{He}} \approx \alpha_{n+1}$. For the n -th energy level the normalization coefficient is given by

$$\begin{aligned} \frac{1}{C_n^2} &= \int_0^{\infty} dz \left[\left| \text{Ai}\left(\frac{z}{z_0} - \alpha_{n+1}^{\text{He}}\right) \right|^2 + \left| \text{Ai}(-\alpha_{n+1}^{\text{He}}) \right|^2 e^{-2\kappa z} \right] \\ &= z_0 \int_0^{\infty} dx \left| \text{Ai}(x - \alpha_{n+1}^{\text{He}}) \right|^2 + \frac{\left| \text{Ai}(-\alpha_{n+1}^{\text{He}}) \right|^2}{2\kappa}. \end{aligned} \quad (19)$$

The first three normalization coefficients are given by $C_0 \approx 1.4261/\sqrt{z_0} \approx 59 \text{ cm}^{-1/2}$, $C_1 \approx 51.3 \text{ cm}^{-1/2}$, $C_2 \approx 47.8 \text{ cm}^{-1/2}$. Using the values $\text{Ai}(-\alpha_1^{\text{He}}) \approx 0.004$, $\text{Ai}(-\alpha_2^{\text{He}}) \approx -0.0045$, and $\text{Ai}(-\alpha_3^{\text{He}}) \approx 0.0048$, this gives $\psi_{\perp 0}(0) \approx 0.236 \text{ cm}^{-1/2}$, $\psi_{\perp 1}(0) \approx -0.231 \text{ cm}^{-1/2}$, $\psi_{\perp 2}(0) \approx 0.23 \text{ cm}^{-1/2}$, etc. These values will be used further below.

In the subsequent sections we consider the stability of a neutron in a bound surface state against various scattering processes. Note that we deal here with a rather unfamiliar scattering problem in that the kinetic energy of the neutron parallel to the surface may be many orders of magnitude greater than the binding energies in the perpendicular direction. We calculate the temperature-dependent scattering rates w_{vap} , w_{rip} and w_{sur} due to ^4He atoms in the vapour above the surface, due to waves on the helium surface, called ripplons, and due to excitations called surfons, respectively.

III. SCATTERING OF NEUTRONS IN SURFACE STATES BY HELIUM VAPOR

^4He vapor atoms can be considered as point-like impurities with interaction potential given by Eq. (1). The momentum distribution of the vapor atoms is given by the Bose distribution [37],

$$N_P = \exp\left(\frac{\mu - E_{\text{He}}}{k_B T}\right), \quad (20)$$

where $k_B = 1.38 \times 10^{-16}$ erg/K is the Boltzmann constant, $\mu/k_B = -7.17$ K is the chemical potential of liquid ^4He (evaporation energy of a ^4He atom) for $T \rightarrow 0$, and $E_{\text{He}} = \mathbf{P}^2/2M$ is the kinetic energy of a ^4He atom with momentum \mathbf{P} . The total atom concentration in the vapor is given by the integrated momentum distribution, i.e.

$$N_{\text{vap}} = \left(\frac{M k_B T}{2\pi\hbar^2}\right)^{3/2} \exp\left(\frac{\mu}{k_B T}\right), \quad (21)$$

where $M = 6.7 \times 10^{-24}$ g is the atomic ^4He mass. Because of the energy-momentum conservation, the neutron scattering rate depends on the initial neutron state and on ^4He atom momentum. We assume the initial neutron state to be given by the lowest energy level along the z -axis and by the momentum $\mathbf{p}_{\parallel} = \{p_x, p_y\}$ parallel to the helium surface, corresponding to the total neutron energy

$$K = p_{\parallel}^2/2m + E_0. \quad (22)$$

In typical experiments with UCN, $K \approx p_{\parallel}^2/2m \sim 10^{-7}$ eV $\gg E_0 \sim 10^{-12}$ eV. The typical initial momentum \mathbf{P} of a He atom is larger than the neutron momentum by still more than one order of magnitude, because its average kinetic energy $\bar{E}_{\text{He}} = (3/2)k_B T \sim 10^{-4}$ eV. Below [see Eq. (34)] we will see that, as $p_{\parallel} \rightarrow 0$, the neutron-He scattering rate w_{vap} remains finite, and we can neglect $p_{\parallel}/P \ll 1$ in the calculation of this rate.

A. Matrix elements

The initial neutron wave function is given by Eqs. (5), (6) and (9). Since the typical neutron out-of-plane kinetic energy after scattering by a He atom of the vapor is much larger than E_0 , and mostly even larger than V_0 given in Eq. (2), the final neutron wave function is close to the three-dimensional plane wave with momentum \mathbf{p}' , normalized to one particle in the whole volume V :

$$\psi' = \exp(i\mathbf{p}'\mathbf{r}/\hbar) / \sqrt{V}. \quad (23)$$

The initial He-atom wave function is $\Psi = \exp(i\mathbf{P}\mathbf{r}/\hbar)$, and the final He wave function is $\Psi' = \exp(i\mathbf{P}'\mathbf{r}/\hbar)$. The

matrix element of the interaction potential (1) is given by

$$\begin{aligned} T_{\text{if}} &= \int d^3\mathbf{r} \psi_{\perp 0}(z) \psi_{\parallel}(\mathbf{r}_{\parallel}) \psi'(\mathbf{r}) \times \\ &\quad \int d^3\mathbf{R} \exp\left(\frac{i(\mathbf{P} - \mathbf{P}')\mathbf{R}}{\hbar}\right) U \delta^{(3)}(\mathbf{r} - \mathbf{R}) \\ &= U \int \frac{d^3\mathbf{R}}{\sqrt{SV}} \psi_{\perp 0}(z_{\text{He}}) \exp\left(\frac{i\Delta\mathbf{P}_{\text{tot}}\mathbf{R}}{\hbar}\right), \end{aligned} \quad (24)$$

where $\Delta\mathbf{P}_{\text{tot}} \approx \mathbf{P} - \mathbf{P}' + \mathbf{p}_{\parallel} - \mathbf{p}'$ is the change of total momentum, \mathbf{R} is the coordinate of the He nucleus, and $\psi_{\perp 0}(z) = C_0 \text{Ai}[(z - E_0/mg)/z_0]$ according to Eq. (9). Introducing $\tilde{u} \equiv z/z_0$ and performing the integration over $d^2\mathbf{R}_{\parallel}$ in Eq. (24) using the identity

$$\int d^2\mathbf{R}_{\parallel} \exp(i\Delta\mathbf{P}_{\text{tot}\parallel}\mathbf{R}_{\parallel}/\hbar) = (2\pi\hbar)^2 \delta^{(2)}(\Delta\mathbf{P}_{\text{tot}\parallel}), \quad (25)$$

one can rewrite T_{if} as

$$T_{\text{if}} = \frac{U (2\pi\hbar)^2 \delta^{(2)}(\Delta\mathbf{P}_{\text{tot}\parallel})}{\sqrt{SV/z_0}} I, \quad (26)$$

where the remaining integral is

$$I \equiv 1.4261 \int_0^{\infty} d\tilde{u} \text{Ai}(\tilde{u} - \alpha_1) \exp\left(\frac{i\Delta p_z \tilde{u}}{\hbar/z_0}\right).$$

We calculate this integral approximately by replacing the normalized Airy function $f(\tilde{u}) \equiv 1.4261 \text{Ai}(\tilde{u} - \alpha_1)$ by a simpler form, also normalized, that is a close approximation, i.e. $f(\tilde{u}) \approx \exp[-(\tilde{u} - \tilde{u}_0)^2/2]/\pi^{1/4}$, where $\tilde{u}_0 \approx 1.5$. Then,

$$\begin{aligned} I &= \int_0^{\infty} d\tilde{u} f(\tilde{u}) \exp\left(\frac{i\Delta p_z \tilde{u}}{\hbar/z_0}\right) \\ &\approx \int_{-\infty}^{\infty} \frac{d\tilde{u}}{\pi^{1/4}} \exp\left[-\frac{(\tilde{u} - \tilde{u}_0)^2}{2} + \frac{i\Delta p_z \tilde{u}}{\hbar/z_0}\right] \\ &= \pi^{1/4} \sqrt{2} \exp\left[\frac{i\Delta p_z \tilde{u}_0}{\hbar/z_0} - \frac{1}{2} \left(\frac{\Delta p_z}{\hbar/z_0}\right)^2\right]. \end{aligned} \quad (27)$$

Below we need only the square of the absolute value of the matrix element T_{if} . The square of the δ -function in $|T_{\text{if}}|^2$ should be treated as

$$\left[(2\pi\hbar)^2 \delta^{(2)}(\Delta\mathbf{P}_{\text{tot}\parallel})\right]^2 = S (2\pi\hbar)^2 \delta^{(2)}(\Delta\mathbf{P}_{\text{tot}\parallel}), \quad (28)$$

because it comes from the extra integration over the coordinate $\mathbf{r}_{i\parallel}$: $\int d^2\mathbf{r}_{i\parallel} = S$. Indeed, substituting Eq. (25) to the l.h.s. of Eq. (28) we obtain

$$\begin{aligned} &(2\pi\hbar)^2 \delta^{(2)}(\Delta\mathbf{P}_{\text{tot}\parallel}) \int d^2\mathbf{r}_{i\parallel} \exp\left(\frac{i\Delta\mathbf{P}_{\text{tot}\parallel}\mathbf{r}_{i\parallel}}{\hbar}\right) = \\ &= (2\pi\hbar)^2 \delta^{(2)}(\Delta\mathbf{P}_{\text{tot}\parallel}) \int d^2\mathbf{r}_{i\parallel} = S (2\pi\hbar)^2 \delta^{(2)}(\Delta\mathbf{P}_{\text{tot}\parallel}). \end{aligned}$$

Substituting Eq. (27) to Eq. (26) and using Eq. (28), we obtain

$$|T_{\text{if}}|^2 \approx \frac{U^2 (2\pi\hbar)^3 \delta^{(2)}(\Delta\mathbf{P}_{\text{tot}||})}{V\sqrt{\pi}\hbar/z_0} \exp\left[-\left(\frac{\Delta p_z}{\hbar/z_0}\right)^2\right].$$

Since $\hbar/z_0 \ll P$, using the identity

$$\delta(x) = \lim_{\epsilon \rightarrow 0} \left[\frac{1}{\epsilon\sqrt{\pi}} \exp\left(-\frac{x^2}{\epsilon^2}\right) \right],$$

we rewrite $|T_{\text{if}}|^2$ as

$$|T_{\text{if}}|^2 \approx U^2 (2\pi\hbar)^3 \delta^{(3)}(\Delta\mathbf{P}_{\text{tot}})/V. \quad (29)$$

B. Scattering rate

The scattering rate of a neutron with initial in-plane momentum $\mathbf{p}_{||}$ by a He atom with initial momentum \mathbf{P} is given by the square of the matrix element (29) integrated over the final momenta \mathbf{p}' and \mathbf{P}' of the neutron and He atom, respectively (Fermi's golden rule [38]):

$$w_{\mathbf{P}} = \frac{2\pi}{\hbar} \int \frac{d^3\mathbf{P}'}{(2\pi\hbar)^3} \int \frac{V d^3\mathbf{p}'}{(2\pi\hbar)^3} |T_{\text{if}}|^2 \delta(\varepsilon - \varepsilon'). \quad (30)$$

Here $\varepsilon \approx P^2/2M$ and $\varepsilon' = P'^2/2M + (\mathbf{p} - \mathbf{p}')^2/2m$ are the initial and final total energies of He-atom and neutron. The scattering rate is approximately independent of the initial neutron momentum $\mathbf{p}_{||}$, i.e., $w_{\mathbf{P}} \equiv w(\mathbf{p}_{||}, \mathbf{P}) \approx w(\mathbf{P})$, because $p_{||} \ll P$ can be neglected in Eq. (30). We now substitute Eq. (29) to Eq. (30). The integration over \mathbf{p}' cancels $\delta^{(3)}(\Delta\mathbf{P}_{\text{tot}})$ in Eq. (29), where $\Delta\mathbf{P}_{\text{tot}} \approx \mathbf{P} - \mathbf{P}' - \mathbf{p}'$. After the integration over the angle ϕ between \mathbf{P} and \mathbf{P}' we obtain

$$w_{\mathbf{P}} = \int \frac{P'^2 dP'}{2\pi\hbar^4} \frac{mU^2}{PP'} \times \theta \left[2PP' - \left| P^2 \left(1 - \frac{m}{M}\right) + P'^2 \left(1 + \frac{m}{M}\right) \right| \right]. \quad (31)$$

Using $M \approx 4m$, from Eq. (31) we obtain

$$w_{\mathbf{P}} \approx \int \frac{P'^2 dP'}{2\pi\hbar^4} \frac{mU^2}{PP'} \theta [8PP' - 3P^2 - 5P'^2]. \quad (32)$$

The integrand is nonzero when the inequality

$$5P'^2 - 8PP' + 3P^2 < 0 \quad (33)$$

is satisfied. The quadratic expression has two real roots, $P' = P(4 \pm 1)/5$, so that Eq. (33) is satisfied for $3/5 < P'/P < 1$, thus defining the range of integration in Eq. (32), i.e.

$$w_{\mathbf{P}} = \int_{3P/5}^P \frac{P' dP'}{2\pi\hbar^4} \frac{mU^2}{P} = \frac{U^2 P m}{2\pi\hbar^4} \frac{8}{25}. \quad (34)$$

Finally, to obtain the total scattering rate as function of temperature one has to integrate Eq. (34) over the initial He-atom momentum \mathbf{P} , weighted with the distribution function N_P of He vapor given by Eq. (20),

$$\begin{aligned} w_{\text{vap}}(T) &= \int \frac{d^3\mathbf{P}}{(2\pi\hbar)^3} N_P w_{\mathbf{P}} \\ &= \int \frac{P^2 dP^2}{(2\pi\hbar)^3} \frac{U^2}{\hbar^4} \frac{8m}{25} \exp\left(\frac{\mu - P^2/2M}{k_B T}\right). \end{aligned}$$

Introducing the new dimensionless variable $P^2/2Mk_B T$ and performing the integration we obtain

$$w_{\text{vap}}(T) = \frac{(2Mk_B T)^2}{(2\pi\hbar)^3} \frac{U^2}{\hbar^4} \frac{8m}{25} \exp\left(\frac{\mu}{k_B T}\right). \quad (35)$$

After substitution of Eq. (1) one obtains

$$w_{\text{vap}}(T) = 9.44 \text{ s}^{-1} \times (T [\text{K}])^2 \times \exp\left(\frac{-7.17}{T [\text{K}]}\right). \quad (36)$$

Hence, $w_{\text{vap}}(1 \text{ K}) \approx 0.007 \text{ s}^{-1} = (138 \text{ s})^{-1}$, and the estimated mean scattering time of a neutron in the lowest level, as determined by He vapor only, is about 138 s at $T = 1 \text{ K}$. Lowering the temperature diminishes the scattering rate more rapid than exponentially, e.g., $w_{\text{vap}}(T = 0.8 \text{ K}) \approx 7.74 \times 10^{-4} \text{ s}^{-1} = (21.53 \text{ min})^{-1}$, and $w_{\text{vap}}(T = 0.7 \text{ K}) \approx 1.6 \times 10^{-4} \text{ s}^{-1}$. The break-even with neutron decay is thus reached slightly above 0.8 K.

IV. SCATTERING FROM SURFACE WAVES

A. General information about ripples

A quantum of a surface wave (ripplon) with momentum \mathbf{q} induces a surface deformation along the z -axis, given by

$$\xi(\mathbf{r}_{||}, t) = \xi_{0q} \sin(\mathbf{q}\mathbf{r}_{||} - \omega_q t). \quad (37)$$

The dispersion relation of surface waves is given by [30, 39]

$$\omega_q^2 = \frac{\alpha}{\rho} (q^2 + \varkappa^2) q \tanh(qd), \quad (38)$$

where $\alpha \approx 0.354 \text{ dyn/cm}$ is the surface tension coefficient of superfluid ^4He , $\rho \approx 0.145 \text{ g/cm}^3$ is its mass density, d is the depth of the helium bath above a horizontal bottom wall, and $\varkappa^2 = (g + f)\rho/\alpha$ with an additional force $f \propto d^{-4}$ due to the van-der-Waals attraction of helium to the bottom wall. The ripplon amplitude ξ_{0q} in Eq. (37), normalized to one ripplon per surface area S , is given by [30, 40, 41]

$$\xi_{0q} = \left(\frac{\hbar q \tanh(qd)}{2S \rho \omega_q} \right)^{1/2}. \quad (39)$$

For a helium bath (in fact already for a thick helium film), $\varkappa = \sqrt{g\rho/\alpha} \approx 20 \text{ cm}^{-1}$. The thermal ripples with energy $\hbar\omega_q \approx k_B T \approx 0.5 \text{ K}$ have the wave number $q \approx 1.2$

nm^{-1} , for which holds $q \gg \varkappa$ and $qd \gg 1$. Then the dispersion relation of riplons is just the dispersion of capillary waves:

$$\omega_q \approx \sqrt{\alpha/\rho} q^{3/2}, \quad (40)$$

and

$$\xi_{0q} \approx \left(\frac{\hbar}{2S\sqrt{\rho\alpha q}} \right)^{1/2}. \quad (41)$$

B. Interaction Hamiltonian

To determine the influence of a periodic surface deformation on the neutron quantum state on the surface we have to separate two limits. The first, *adiabatic* limit appears when the surface oscillates so slowly that the neutron wave function adjusts to the instantaneous surface profile. The interaction potential in this limit is found in Appendix A, see Eq. (A8), and can be rewritten as

$$\hat{H}_{\text{int}} = \xi(\mathbf{r}_{\parallel}, t) \left\{ \left[\frac{(\hat{p}_{\parallel} + \hat{p}_q)^2 - \hat{p}_{\parallel}^2}{2m} - \hbar\omega_q \right] \frac{\partial}{\partial z} + mg \right\}, \quad (42)$$

where $\hat{p}_{\parallel} = -i\hbar\nabla_{\parallel}$ and $\hat{p}_q = \hbar q$ are the momentum operators of the neutron and ripplon along the surface, respectively. This interaction term generalizes Eq. (7) of Ref. [28], because it does not exclude coordinate-dependent surface perturbations. The expression in the square brackets in Eq. (42) is just the transfer of the total (neutron+riplon) kinetic energy to the final neutron kinetic energy along the z -axis.

The opposite, anti-adiabatic or *diabatic* limit appears when the surface oscillates much faster than the characteristic frequency of the out-of-plane neutron motion, so that the neutron wave function does not adjust to the instantaneous surface profile. In this limit a surface wave affects the neutrons by creating an additional time- and coordinate-dependent periodic potential

$$V_r(\mathbf{r}_{\parallel}, z) = \begin{cases} V_0 & \text{at } 0 < z < \xi(\mathbf{r}_{\parallel}, t) \text{ for } \xi(\mathbf{r}_{\parallel}, t) > 0 \\ -V_0 & \text{at } \xi(\mathbf{r}_{\parallel}, t) < z < 0 \text{ for } \xi(\mathbf{r}_{\parallel}, t) < 0 \end{cases}. \quad (43)$$

The ripplon amplitude, given by Eqs. (39) or (41), for any reasonable value of S is much less than the atomic scale and, even more, than the typical scale of the neutron wave function, given by $\kappa_0^{-1} \approx 33 \text{ nm}$ at $z < 0$ [Eq. (8)]. Therefore, the potential in Eq. (43) can be approximated by

$$V_r(\mathbf{r}) \equiv V_r(\mathbf{r}_{\parallel}, z) \approx V_0 \xi(\mathbf{r}_{\parallel}, t) \delta(z). \quad (44)$$

C. Crossover between adiabatic and diabatic limits and matrix elements

The diabatic-adiabatic crossover, corresponding to a change of the ripplon-neutron interaction Hamiltonian

from Eq. (43) to Eq. (42), must take place when the ripplon frequency ω_q and the wave-vector \mathbf{q} decrease. However, the estimate of the crossover frequency ω_{qc} and the description of the system in the crossover regime is not a trivial problem. Similar problem appears in other condensed-matter systems and requires a special theoretical study (see, e.g., Refs. [42–46]).

One may, naively, define the crossover as the region where the ripplon frequency becomes comparable to the quasi-classical bouncing frequency of a neutron in the ground level in z -direction, i.e. when the ratio $\hbar\omega_q/E_0 \sim 1$, where E_0 given by Eq. (13). This corresponds to the ripplon frequency

$$\omega_{qc} \sim E_0/\hbar = 915 \text{ s}^{-1}, \quad (45)$$

and to the ripplon wave number

$$q_c \approx (\omega_{qc}^2 \rho / \alpha)^{1/3} = 70 \text{ cm}^{-1} > \varkappa. \quad (46)$$

However, such an estimate of the diabatic-adiabatic crossover has an important drawback: it does not depend on the value V_0 of the neutron potential inside helium. Generally, we expect that for $V_0 \rightarrow 0$ and for non-zero q and ω_q one can always apply Eq. (43), and for $V_0 \rightarrow \infty$ one can always apply Eq. (42), which contradicts Eq. (45). The classical definition of the diabatic-adiabatic crossover, given by Eqs. (B5) and (B6) in Appendix B, has the same drawback.

A rigorous analysis of the adiabatic/diabatic crossover should be based on the solution of the Schrödinger equation for a neutron in the time-dependent potential given by Eqs. (A1) and (A2). One may approximately determine the criterion of adiabatic/diabatic crossover from the variational principle to minimize the neutron energy. This approach would be definitely correct for a time-independent potential. The lowest-level out-of-plane neutron wave function is chosen to minimize the neutron energy. In the adiabatic limit the energy loss is the kinetic and gravitational energy from Eq. (42), while in the diabatic limit it is the potential energy from Eq. (43). The first-order energy correction is given by the diagonal matrix elements of these two interaction potentials, or more precisely by the Hamiltonian in Eq. (A2). If these diagonal matrix elements are nonzero, their comparison gives the crossover frequency. If these matrix elements vanish in the first order in ξ , one needs to calculate and compare the second-order corrections. Since $\int_{-\infty}^{\infty} dz \psi_{\perp 0}^*(z) \partial \psi_{\perp 0}(z) / \partial z = 0$, and $\int \xi(\mathbf{r}_{\parallel}, t) d^2 \mathbf{r}_{\parallel} = 0$, the first-order (in ξ) diagonal matrix element of the adiabatic Hamiltonian in Eq. (42) vanishes. So does the diagonal matrix element of the diabatic Hamiltonian in Eq. (43) in the first-order in ξ , if $\mathbf{p}_{\parallel} \neq \hbar \mathbf{q}$. Hence, to calculate the crossover frequency one needs to calculate the second-order energy corrections, which do not vanish. These corrections are determined, in particular (but not only), by the matrix elements of the neutron-riplon interaction potentials in Eqs. (42) and (43). Therefore, for an estimate of the position (riplon frequency) of the

adiabatic/diabatic crossover the comparison of the matrix elements, given below, is more accurate than just the comparison of ripplon frequency with E_0 . As we will see, the final result of the neutron-riplon scattering rate is not sensitive to this crossover frequency, because the main contribution to this scattering rate comes from the riplons with energy $\hbar\omega_q \sim V_0 \gg \hbar\omega_{qc}$, which corresponds to the far diabatic limit.

Therefore, a rough estimate of the crossover between diabatic and adiabatic limits is given by the ripplon frequency when two interaction Hamiltonians, given by Eqs. (43) and (42), become of the same order of magnitude. More precisely, we compare their matrix elements for the neutron transitions between lowest energy levels of their motion in z -direction. Thus defined, the diabatic-adiabatic crossover depends on V_0 and meets other general requirements, such as the adiabatic limit for $\omega_q, q \rightarrow 0$. The matrix element T_{if} of the diabatic interaction potential in Eq. (44) for the transitions between two neutron states with initial wave function $\psi_{\perp}(z)$ and final wave function $\psi'_{\perp}(z)$, written explicitly in Eqs. (5)-(9), is given by

$$T_{\text{if}} = \int \frac{d^3\mathbf{r}}{S} \psi_{\perp}(z) \psi'_{\perp}(z) \exp\left(i\mathbf{r}_{\parallel} \frac{\mathbf{p}_{\parallel} - \mathbf{p}'_{\parallel}}{\hbar}\right) V_0 \xi(\mathbf{r}_{\parallel}) \delta(z).$$

The integral over z cancels $\delta(z)$, while after substituting Eq. (37) the integration over \mathbf{r}_{\parallel} gives $(2\pi\hbar)^2 \delta^{(2)}(\Delta\mathbf{p}_{\text{tot}\parallel})$, where $\Delta\mathbf{p}_{\text{tot}\parallel} = \hbar\mathbf{q} + \mathbf{p}_{\parallel} - \mathbf{p}'_{\parallel}$ is the change of the total in-plane momentum of the ripplon+neutron system. As a result we obtain

$$T_{\text{if}} = V_{\parallel} V_{0,n}. \quad (47)$$

The factor

$$V_{\parallel} = S^{-1} (2\pi\hbar)^2 \delta^{(2)}(\Delta\mathbf{p}_{\text{tot}\parallel}) \quad (48)$$

is due to the in-plane part $\psi_{\parallel}(\mathbf{r}_{\parallel})$ of the neutron wave function, given by Eq. (6), and

$$V_{0,n} = V_0 \xi_{0q} \psi_{\perp 0}^*(0) \psi_{\perp n}(0) \quad (49)$$

comes from its out-of-plane part $\psi_{\perp}(z)$. The squared modulus of the matrix element in Eq. (47) follows as

$$|T_{\text{if}}|^2 = \frac{(2\pi\hbar)^2 \delta^{(2)}(\Delta\mathbf{p}_{\text{tot}\parallel})}{S} |\psi_{\perp}(0) \psi'_{\perp}(0) V_0 \xi_{0q}|^2, \quad (50)$$

where we again have used Eq. (28).

The matrix elements of the adiabatic interaction potential in Eq. (42) for $\xi(\mathbf{r}_{\parallel}, t)$ given by Eq. (37) are

$$\hat{H}_{k,n} = V_{\parallel} \xi_{0q}(E_k - E_n) Q_{k,n}, \quad (51)$$

where V_{\parallel} is again given by Eq. (48) and

$$Q_{k,n} = \int_0^{\infty} dz \psi_{\perp k}^*(z) \frac{d\psi_{\perp n}^*(z)}{dz}. \quad (52)$$

The first values of $Q_{k,n}$ are given in Table I of Ref. [28], e.g., $Q_{0,1} = 0.09742 \mu\text{m}^{-1}$, $Q_{0,2} = -0.05355 \mu\text{m}^{-1}$, $Q_{0,3} = 0.03831 \mu\text{m}^{-1}$, $Q_{0,4} = -0.0304 \mu\text{m}^{-1}$. Substituting these values we obtain for the first levels the ratio $V_{0,n}/\hat{H}_{0,n} \approx 1$ at

$$\omega_{qc} \approx 10^3 \text{ s}^{-1}. \quad (53)$$

By chance, the diabatic-adiabatic crossover condition, defined as $V_{0,n} \sim \hat{H}_{0,n}$, is close to the value quoted in Eq. (45).

Below, we consider mainly the neutron-riplon interaction in the diabatic limit, corresponding to the ripplon frequency $\omega_q > \omega_{qc}$ and the interaction potential given by Eq. (44), because it deals with much larger phase space of riplons and because, as we will see later, the main contribution to the neutron-riplon scattering rate comes from the riplons with energy $\hbar\omega_q \sim V_0 \gg \hbar\omega_{qc}$.

The scattering rate w_{rip} of a neutron with initial in-plane momentum \mathbf{p}_{\parallel} on riplons is determined by two processes: the absorption and the emission of a ripplon with wave vector \mathbf{q} and energy $\hbar\omega_q$,

$$w_{\text{rip}} = w_{\text{abs}} + w_{\text{em}}. \quad (54)$$

Since for typical ^4He temperatures $k_{\text{B}}T$ is much larger than the initial neutron energy K , the populations of ripplon states with relevant energies are $N_q \gtrsim 1$ or even $N_q \gg 1$. The phase volume of an absorbed ripplon is much larger than that of an emitted ripplon, because the energy of the latter is limited to the initial kinetic energy of the neutron, $K \ll k_{\text{B}}T$. Hence, one could expect that the ripplon-neutron scattering rate is dominated by ripplon absorption, so that $w_{\text{rip}} \approx w_{\text{abs}}$. However, because of a low-energy divergence of w_{rip} (see below), the emission of low-energy riplons with energies $\hbar\omega_q \ll K$ may also be important, and we therefore consider both these processes.

D. Absorption of riplons

The absorption scattering rate w_{abs} of a neutron with initial in-plane momentum \mathbf{p}_{\parallel} in the discrete vertical level with energy E_0 is given by Fermi's golden rule,

$$w_{\text{abs}} = \frac{2\pi}{\hbar} \int \frac{N_q S d^2\mathbf{p}_q}{(2\pi\hbar)^2} \int \frac{S d^2\mathbf{p}'_{\parallel}}{(2\pi\hbar)^2} \sum_n |T_{\text{if}}|^2 \delta(\varepsilon - \varepsilon'), \quad (55)$$

where $\mathbf{p}_q \equiv \hbar\mathbf{q}$ is the ripplon momentum, and \mathbf{p}'_{\parallel} and n are the in-plane momentum and out-of-plane quantum number of the final neutron state, respectively.

$$N_q = [\exp(\hbar\omega_q/k_{\text{B}}T) - 1]^{-1} \quad (56)$$

is the Bose distribution function of riplons with energy $\hbar\omega_q$ and with zero chemical potential. The matrix element $|T_{\text{if}}|^2$ is given by Eq. (50) and the initial total energy by

$$\varepsilon = \hbar\omega_q + \mathbf{p}_{\parallel}^2/2m + E_0. \quad (57)$$

The final energy $\varepsilon' = \mathbf{p}'_{\parallel}^2/2m + E_n$, after using the in-plane momentum conservation expressed by the δ -function in Eq. (50), can be rewritten as

$$\varepsilon' = \frac{p_{\parallel}^2 + p_q^2 + 2p_q p_{\parallel} \cos \phi}{2m} + E_n, \quad (58)$$

where ϕ is the angle between \mathbf{p}_{\parallel} and \mathbf{p}_q . The integration over the component \mathbf{p}'_{\parallel} of the final neutron momentum parallel to the surface cancels the δ -function in Eq. (50). After substitution of Eqs. (50), (57) and (58) to Eq. (55) we obtain

$$w_{\text{abs}} = \int \frac{N_q S p_q d p_q d \phi}{2\pi \hbar^3} \sum_n |\psi_{\perp 0}(0) \psi_{\perp n}^*(0) V_0 \xi_{0q}|^2 \times \delta \left(\hbar \omega_q - \Delta E_n - \frac{p_q^2 + 2p_q p_{\parallel} \cos \phi}{2m} \right), \quad (59)$$

where $\Delta E_n = E_n - E_0 \approx E_n$ is the change of the out-of-plane neutron energy after the ripplon absorption. The integration over ϕ cancels the δ -function in Eq. (59) and gives

$$w_{\text{abs}} = \int_0^{\infty} \frac{N_q S p_q d p_q}{\pi \hbar^3} \sum_n \frac{|\psi_{\perp 0}(0) \psi_{\perp n}^*(0) V_0 \xi_{0q}|^2}{\sqrt{a^2 - (b - \Delta E_n)^2}}, \quad (60)$$

where $a \equiv p_{\parallel} p_q / m$ and $b \equiv \hbar \omega_q - p_q^2 / 2m$. [80] We estimate this integral in the Appendix C. This calculation gives the upper estimate of w_{abs} [see Eqs. (C11), (C17) and (C21)] of

$$w_{\text{abs}}^{\text{up}} \approx w_{>}^{\text{up}} + w_{<}^{\text{up}} + w_{\ll}^{\text{up}} \approx 7 \times 10^{-5} \times T [\text{K}] \text{ s}^{-1}. \quad (61)$$

This corresponds to a mean neutron scattering time due to ripplon absorption of $\tau_{\text{rip}} > 4$ hours even at $T = 1$ K.

E. Emission of ripples

The rate of emission of a ripplon by a surface-state neutron with momentum \mathbf{p}_{\parallel} is given by Fermi's golden rule, similar to Eq. (55):

$$w_{\text{em}} = \frac{2\pi}{\hbar} \int \frac{N'_q S d^2 \mathbf{p}_q}{(2\pi \hbar)^2} \int \frac{S d^2 \mathbf{p}'}{(2\pi \hbar)^2} \sum_n |T_{\text{if}}|^2 \delta(\varepsilon - \varepsilon'). \quad (62)$$

Here, $\mathbf{p}_q \equiv \hbar \mathbf{q}$ is now the emitted-riplon momentum, $\mathbf{p}' = \mathbf{p}_{\parallel} - \mathbf{p}_q$ is the in-plane neutron momentum after emission of the ripplon,

$$N'_q = 1 + [\exp(\hbar \omega_q / k_B T) - 1]^{-1}, \quad (63)$$

is the ripplon population, $\varepsilon \approx \mathbf{p}_{\parallel}^2 / 2m$ is the initial total energy, and

$$\varepsilon' = \frac{p_{\parallel}^2 + p_q^2 - 2p_q p_{\parallel} \cos \phi}{2m} + E_n + \hbar \omega_q,$$

is the final total energy. The matrix element is given by Eq. (50). The integration over \mathbf{p}' in Eq. (62) cancels the δ -function in the matrix element,

$$w_{\text{em}} = \int \frac{S N'_q p_q d p_q}{2\pi \hbar^3} \sum_n |\psi_{\perp}(0) \psi_{\perp}^*(0) V_0 \xi_{0q}|^2 \times \int_0^{2\pi} d\phi \delta \left(\frac{p_q^2 - 2p_q p_{\parallel} \cos \phi}{2m} + E_n + \hbar \omega_q \right) \quad (64)$$

The integration over the angle ϕ between \mathbf{p}_{\parallel} and \mathbf{p}_q in Eq. (64) is similar to that in the preceding subsection in Eq. (59) and gives

$$w_{\text{em}} = \int_0^{p_{\text{em}}^{\text{max}}} \frac{S N_q p_q d p_q}{\pi \hbar^3} \sum_n \frac{|\psi_{\perp}(0) \psi_{\perp}^*(0) V_0 \xi_{0q}|^2}{\sqrt{a^2 - (b_1 + \Delta E_n)^2}}, \quad (65)$$

where $a \equiv p_{\parallel} p_q / m$ as in the previous subsection, and $b_1 = \hbar \omega_q + p_q^2 / 2m$. The integrand is real when $0 \leq \Delta E_n \approx E_n \leq a - b_1 = p_{\parallel} p_q / m - \hbar \omega_q - p_q^2 / 2m$. This can be satisfied when $a - b_1 > 0$, which for $p_{\parallel}^2 / 2m = 100$ neV gives $p_q < p_{\text{em}}^{\text{max}} = \hbar q_{\text{em}}^{\text{max}}$ with $q_{\text{em}}^{\text{max}} \approx 6.5 \times 10^4 \text{ cm}^{-1}$. The maximum value of $a - b_1$ is ~ 3 neV $\ll V_0 = 18.5$ neV. Hence, for the emission of ripples, $E_n \ll V_0$, and we may use Eqs. (13), (15) and (C18). In addition, instead of three intervals of parameters for the ripplon absorption, we only need to consider one interval. Substituting Eqs. (40), (41) and the upper estimate of $|\psi'_{\perp}(0)|^2 \leq |\psi_{\perp 0}(0)|^2$ to Eq. (65), we obtain an upper estimate $w_{\text{em}}^{\text{up}}$ for w_{em} :

$$w_{\text{em}}^{\text{up}} \approx \int_0^{p_{\text{em}}^{\text{max}}} \frac{k_B T p_q d p_q}{2\pi \hbar \alpha p_q^2} \int \frac{dn |\psi_{\perp 0}^2(0) V_0|^2}{\sqrt{a^2 - (b_1 + E_n)^2}} \quad (66)$$

$$= \int \frac{k_B T d p_q}{\pi^2 \hbar^2 \alpha p_q} \frac{|\psi_{\perp 0}^2(0) V_0|^2}{g \sqrt{2m}} \int_0^{a-b_1} \frac{\sqrt{E_n} d E_n}{\sqrt{a^2 - (b_1 + E_n)^2}}.$$

This integral resembles the one in Eq. (C19): the only difference is the sign of E_n in the denominator and, consequently, a different upper integration limit. We may give an upper estimate of this integral by replacing $\sqrt{E_n}$ by its maximum value $\sqrt{a - b_1}$ in the integrand and by replacing the lower limit by $-b_1$ in Eq. (66). This gives

$$w_{\text{em}}^{\text{up}} \approx \int \frac{k_B T d p_q}{\pi^2 \hbar^2 \alpha p_q} \frac{|\psi_{\perp 0}^2(0) V_0|^2}{g \sqrt{2m}} \int_{-b_1}^{a-b_1} \frac{\sqrt{a - b_1} d E_n}{\sqrt{a^2 - (b_1 + E_n)^2}}$$

$$= \int_0^{p_{\text{em}}^{\text{max}}} \frac{k_B T d p_q}{\pi \hbar^2 \alpha p_q} \frac{|\psi_{\perp 0}^2(0) V_0|^2}{2g \sqrt{2m}} \sqrt{\frac{p_{\parallel} p_q}{m} - \hbar \omega_q - \frac{p_q^2}{2m}}.$$

The integral converges. Neglecting $p_q^2 / 2m \ll \hbar \omega_q$ and changing the integration variable to $\sqrt{p_q}$ we finally obtain

$$w_{\text{em}}^{\text{up}} \approx \frac{k_B T}{\pi \hbar^2 \alpha} \frac{|\psi_{\perp 0}^2(0) V_0|^2}{g \sqrt{2m}} \frac{2}{3} \left(\frac{p_{\parallel}}{m} \right)^{3/2} \sqrt{\frac{\rho \hbar}{\alpha}}. \quad (67)$$

The rate of ripplon emission depends on the initial neutron momentum p_{\parallel} . At $K = p_{\parallel}^2/2m = 100$ neV Eq. (67) gives

$$w_{\text{em}}^{\text{up}} \approx 2 \times 10^{-5} \text{ s}^{-1} \times T [\text{K}]. \quad (68)$$

Combining Eqs. (61) and (68) we obtain an upper estimate for the total scattering rate of a surface neutron in the lowest energy level E_0 by riplons:

$$w_{\text{rip}}^{\text{up}} = w_{\text{abs}}^{\text{up}} + w_{\text{em}}^{\text{up}} \approx 9 \times 10^{-5} \text{ s}^{-1} \times T [\text{K}]. \quad (69)$$

This rate corresponds to a mean neutron scattering time due to the riplons of $\tau_{\text{rip}} > 3$ hours even at $T = 1$ K.

V. OTHER NEUTRON SCATTERING PROCESSES

A. Scattering of surface neutrons by bulk phonons

The scattering of ultra-cold neutrons inside superfluid helium by bulk phonons has been studied in Ref. [47]. There, two main processes were identified: (i) one-phonon absorption and (ii) one-phonon absorption combined with emission of another phonon due to the cubic term in the phonon Hamiltonian. The second process was found to dominate at low temperature, resulting in a total scattering time of about $\tau_{\text{ph0}} = 100$ s for a neutron propagating through liquid ${}^4\text{He}$ at $T = 1$ K. In our case of a neutron above the He surface, both scattering processes are weakened by the factor

$$\int_{-\infty}^0 \psi_{\perp}^2(z) dz = \psi_{\perp}^2(0)/2\kappa \approx 1.16 \times 10^{-7},$$

because only a small part of the neutron wave function penetrates into the liquid helium. Hence, for helium temperatures below 1 K, the neutron scattering time constant due to bulk phonons, $\tau_{\text{ph}} \approx \tau_{\text{ph0}} 2\kappa/\psi_{\perp}^2(0) \gtrsim 10^9$ s, is extremely long and can safely be ignored.

B. Scattering by surfons

Recently, a new type of surface excitation was proposed [48] in addition to the riplons, in order to explain the temperature dependence of the surface tension coefficient of liquid helium. These excitations, called surfons, are He atoms in a quasistationary discrete quantum energy level above the liquid helium surface [48–50]. The state is formed by the combination of the van-der-Waals attractive potential of the bulk helium and the hard-core repulsion between He atoms. Although there is so far only indirect experimental evidence for this type of surface excitation, we consider the neutron-surfon scattering rate to compare with the other processes. The interaction potential is the same as for neutron interaction with the helium vapor, but the surfons propagate only along the helium surface. Therefore, the surfon-neutron interaction

contains an additional small factor $\sim z_0 \psi_{\perp}^2(0) \sim 3 \times 10^{-5}$ due to a small overlap of the neutron and the surfon wave functions. The activation energy of the surfon has been obtained from fitting the temperature dependence of the surface tension coefficient of liquid ${}^4\text{He}$ to the experimental data [49]. Its value, $\Delta_{\text{s0}} \approx k_{\text{B}} \times 2.67 \text{ K} = 3.7 \times 10^{-16}$ erg, is significantly smaller than the evaporation energy $-\mu = k_{\text{B}} \times 7.17 \text{ K}$ of a ${}^4\text{He}$ atom. Therefore, at low enough temperature the neutron scattering by surfons will exceed the scattering rate on helium vapor and must be considered for completeness.

In the calculation we can neglect the initial UCN momentum p as compared to the large surfon initial momentum $P_{\parallel} \sim \sqrt{2k_{\text{B}}T M}$, similarly to our treatment of the scattering from helium vapor in Sec. III. We also assume that the surfon in-plane kinetic energy is not sufficient to evaporate the He atom from the surfon state after scattering. The vertical neutron energy level E_n may change, however, and the out-of-plane neutron momentum may not be conserved because the helium surface violates the spatial uniformity along the z -axis. The surfon energy consists of the excitation energy Δ_{s0} and of the kinetic energy $K_{\text{sur}} = P_{\parallel}^2/2M$ of its in-plane motion. The populations of the surfon states are approximately given by the Boltzmann distribution, $N_{\text{sur}}(P_{\parallel}) \approx \exp\left[-(\Delta_{\text{s0}} + P_{\parallel}^2/2M)/k_{\text{B}}T\right]$. The calculation is described in Appendix D and gives a very small upper estimate for the scattering rate of neutrons on surfons:

$$\begin{aligned} w_{\text{sur}}^{\text{up}} &= \frac{(Mk_{\text{B}}T)^{3/2} a_{\text{He}}^2}{\hbar^2 m} |\psi_{\perp 0}^2(0)| \frac{\sqrt{1.6\pi}}{5} \exp\left(\frac{-\Delta_{\text{s0}}}{k_{\text{B}}T}\right) \\ &\approx 4 \times 10^{-8} \exp\left(\frac{-\Delta_{\text{s0}}}{k_{\text{B}}T}\right) \times T^{3/2} [\text{K}] \text{ s}^{-1}. \end{aligned} \quad (70)$$

Hence, at temperatures $T > 0.25$ K, the neutron scattering rate $w_{\text{sur}}^{\text{up}}$ by surfons is found to become much smaller than the scattering rate w_{vap} by helium vapor given in Eq. (36). However, for this and lower temperatures, the scattering by riplons is dominant, $w_{\text{sur}}^{\text{up}} \ll w_{\text{rip}}^{\text{up}}$, so that scattering of UCNs by surfons is negligibly small at any temperature.

Thus, the total scattering rate w_{tot} of UCNs on the liquid helium surface is determined by the helium vapor at high temperatures $T \gtrsim 0.6$ K, and by riplons at low temperatures $T \lesssim 0.6$ K. It is plotted as function of temperature in Figs. 2 and 3.

VI. DISCUSSION AND SKETCHES OF EXPERIMENTAL IMPLEMENTATIONS

The calculations presented in this paper show that, at temperatures below 0.7 K, the mean scattering time of a neutron in a gravitational quantum state above a horizontal flat surface of liquid helium is greater than the neutron beta-decay lifetime. This surface might therefore indeed represent an almost perfect mirror, which calls for

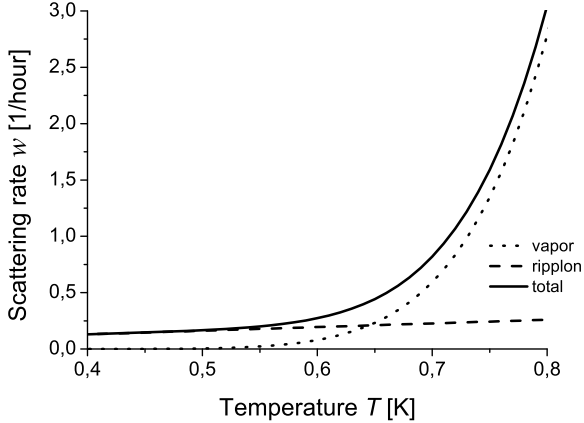


FIG. 2: The calculated total scattering rate (solid line) of UCNs on the liquid helium surface in inverse hours. The dotted and dashed lines give the contributions due to helium vapor and ripples, respectively.

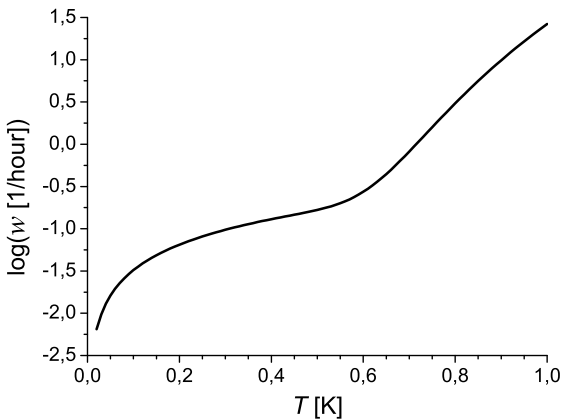


FIG. 3: The logarithm with base 10 of the calculated total scattering rate of UCNs on the liquid helium surface.

experimental demonstration and applications. The system could offer excellent possibilities not only to study the quantum states represented in Fig. 1 but also serve as a sensitive probe for detection of tiny energy transfers due to helium-intrinsic or external perturbations. The application having motivated this theoretical work is a high-precision study of the level scheme of the neutron in the gravitational potential above the liquid mirror, giving access to short-range, gravitation-like interactions between the neutron and the mirror. A motivation from an experimental point of view has been current work on new UCN sources at the ILL [52, 53] which involves cooling many liters of ultrapure, superfluid helium below 0.7 K. The development had been started at the TU Munich [54, 55] and builds on theoretical work by Golub and Pendlebury on superthermal UCN production via down-scattering of cold neutrons in superfluid helium [56, 57].

The scattering rate of neutrons on helium vapor decreases stronger than exponentially while lowering the temperature [$\propto T^2 \exp(-\text{const}/T)$, see Eq. (36)]. Already for 0.8 K it is calculated to be smaller than the neutron decay rate. An upper estimate of the scattering rate due to ripples at 0.8 K is found to be by one order of magnitude lower than the rate due to the vapor. Owing to its linear temperature dependence it will become the dominant contribution below about 0.6 K [see Eq. (69)], however at a level already 50 times below the neutron decay rate. While all processes calculated here should be insignificant for precision studies of the level scheme, experiments involving storage of neutrons with energies up to the cutoff set by the neutron optical potential barrier V_0 of the superfluid helium [see Eq. (2)] may have different requirements. In this respect it seems helpful that the main contribution to the neutron scattering rate at such low temperatures is due to the low-energy part of the ripplon spectrum and thus will dominantly lead only to transitions between nearby neutron quantum states. Energy transfers of a few peV are however usually insufficient to cause a neutron to penetrate through the liquid helium and thus leave the system. Therefore, at 0.6 K the mean escape time of a UCN with initial kinetic energy $K < V_0$ could be longer than the neutron beta-decay lifetime by several orders of magnitude. This makes an experimental set-up using a liquid helium surface a strong candidate for a nearly loss-free neutron container and has indeed been proposed to be applied in a neutron lifetime experiment [58, 59]. For highest reliability, measurements should nonetheless be performed at different temperatures and the container preferentially be filled with a neutron spectrum with a gap between its upper cut-off and V_0 . It should also be noted that the value $V_0 = 18.5$ neV for superfluid helium is small compared to $\gtrsim 100$ neV for conventional materials used for neutron bottles. Counting statistics might therefore become a limiting issue. Still, a neutron lifetime measurement employing a trap involving a horizontal surface of superfluid helium seems an interesting complement to projects employing magnetic neutron traps. While these possess typical trapping potentials for low-field-seeking neutrons in the range (50 – 120) neV and completely avoid any wall collisions of truly trapped neutrons, other systematic effects such as marginally trapped neutrons and depolarization need to be carefully addressed [60–67] (see also Refs. [68, 69] for recent reviews and discussion of the neutron lifetime problem).

Turning to the question how to populate and detect the neutron quantum states above a superfluid-helium mirror (called "lake" in the sequel) one first notes that, in contrast to a solid mirror as employed in previous and ongoing experiments, one has to confine the liquid and deal with the presence of a meniscus at the border of the helium container (the "coast" of the lake). In the traditional "flow-through" scheme of current experiments neutrons enter a mirror table with an absorbing ceiling from one side and are detected on the other side. This might also be tech-

nically feasible for the liquid mirror, where neutrons will then however have to enter and exit the lake through a thin, weakly absorbing foil with low (or negative) neutron optical potential. Application of magnetic fields might offer more attractive, novel experimental possibilities which we sketch below.

Considering first a technique for state population, we note that one may employ a magnetic field gradient for deceleration of neutrons moving from above towards the horizontal mirror located at $z = 0$. Neutrons with magnetic moment μ_n in a magnetic field with modulus B have a potential energy of $\pm |\mu_n| B$, with sign depending on the spin state with respect to the field direction. The upper (lower) sign refers to those neutrons which become repelled (attracted) by a positive gradient of magnetic field modulus. They are correspondingly called low-field (high-field) seekers. Note recent experimental demonstrations of trapped high-field seeking UCNs [70, 71]. A magnetic field modulus $B(z) = Cz$, for instance with constant (positive) gradient $C > mg/|\mu_n| \approx 1.66$ T/m overcompensates gravitation for the high-field seeking neutrons. Those with vertical kinetic energy $E_\perp = (|\mu_n|C - mg)h$ at height h will thus have lost this energy entirely when arriving at the mirror. This situation is analog to a neutron rising in the earth's gravitational field to its apogee (after which it will fall back down). If alternatively, one wants to decelerate the low-field seeking neutrons, the gradient has to be inverted and hence the strongest field needs to be located at the surface. While the neutron is close to the lowest point of its trajectory, the magnetic field gradient nearby the mirror needs to be switched off. For limitation of the spatial region where the field needs to be provided, one may employ a vertical, straight neutron guide, ending above and close to the mirror. A circular absorber with a central hole for the neutron-feeding pipe and mounted with variable distance of some tens of μm above the lake may serve for preparation of low neutron quantum states as used in the first experiments [13]. An obvious benefit of the magnetic population method is a possible neutron detection acceptance angle of the full 2π . Using a helium lake offers the additional advantage that the presumably nearly perfect mirror can be made much larger than the quartz mirrors employed in current experiments.

Compared with a flow-through experiment the sensitivity of the energy state determination may be drastically improved using lateral UCN trapping prior to detection, ideally for many hundreds of seconds. This might be possible using a magnetic fence, consisting of a multipolar magnetic field arrangement similar to the system described in Ref. [72]. For our purpose the multipole of high order has to be oriented such as to provide only field components within the plane defined by the helium surface, i.e., with current-carrying rods parallel to the gravity field. This will keep low-field seeking neutrons away from the liquid meniscus at the container wall, thus keeping the vertical neutron state unaffected. Note that, if one populates the lake with high-field seeking neutrons, their spin has to be flipped after arrival at the surface and prior to ar-

rival in the region of strong multipolar field, which can be done, e.g., using standard magnetic resonance techniques. Detection can still be done through the side walls of the helium container, requiring switching-off of the magnetic fields (or better a spin flip to turn the trapped low-field seeking neutrons into high-field seekers to accelerate them through gaps in the magnetic fence). Alternatively, one may let them rise back to the entrance of the neutron guide by switching on again the magnetic field gradient used for lake population.

Next, we discuss a possible further improvement of the lake population technique, noting first that a vertical straight and specularly reflecting guide with constant cross section does not mix the vertical with the horizontal components of neutron velocity. As a result, the closer a typical neutron approaches the mirror, the larger will be the number of reflections per length unit of the guide. Even a small non-specularity in the reflection will then become an issue. In addition, a typical neutron from a typical UCN source will, after removal of its kinetic energy in the vertical direction, still have a typical final speed parallel to the surface of several meters per second. A lower neutron speed would however be beneficial for both the flow-through mode and for trapping. For the former it increases the time a neutron spends on the mirror, while for the latter a lower magnetic field strength is sufficient for lateral UCN confinement on the lake.

A non-imaging neutron optical device proposed by Hickerson and Filippone offers an interesting remedy for the aforementioned deficiencies of a straight guide [73]. They describe a compound parabolic concentrator (CPC) for neutrons rising from a Lambertian horizontal disk source upwards against the gravitational field. Its neutron-optical properties are based on the "neutron fountain" [74] valid for constant force fields along the symmetry axis of a parabolic reflecting surface. Using a constant magnetic field gradient that overcompensates the effect of gravitation, neutrons approaching the lake from above will experience a constant deceleration $a = C/m - g$. We may thus apply the CPC inverted in space with the neutron source (an aperture with radius R) located at height h above the lake. According to the formulas given in Ref. [73], neutrons starting there at time $t = 0$ and with speed v_0 will, after a time $T = v_R/a$ (where $v_R = \sqrt{v_0^2 + 2aR}$) and with typically fewer than two reflections, arrive within a narrow band of heights $0 \leq z < R$ above the horizontal mirror. The spread of total kinetic energy within the ensemble of UCN is then only $\Delta E \approx maR/3$ and independent of v_0 . After switching off the field gradient, the neutrons close to the mirror will thus move with much reduced lateral velocities compared to the traditional beam method. Hence, even without lateral trapping, state population via a CPC will lead to much increased interaction times with the mirror and a corresponding gain in accuracy of measurements. A CPC will be most beneficial at a pulsed UCN source, preferably in combination with a rebunching technique as demonstrated in Ref. [75], and hence works best in combination with a UCN trapping

experiment. We note that the very low lateral neutron velocities allow for quite modest magnetic trapping fields, which makes it easy to provide large openings for neutron detection in the magnetic fence. Obviously, a CPC with a magnetic deceleration system might also be used for a sufficiently large conventional mirror.

In summary, this paper has given positive answers concerning necessary prerequisites for application of a superfluid-helium mirror for study and application of neutron quantum levels in the Earth gravity field. Further investigations will be needed to address questions on neutron manipulation, e.g., if transitions between levels can be induced by vibrations of the helium surface in a controlled way. It might also be worthwhile to consider further possibilities to create a flat mirror of large surface, such as "Fomblin" oil (a fluorinated, organic compound with low neutron absorption, already tested as part of an optical system for a new neutron charge measurement [76]) or liquid or solid neon.

P. G. thanks A. M. Dyugaev for useful discussions. The work was supported by RFBR grant #13-02-00178.

Appendix A: Derivation of the neutron-ripplon interaction in the adiabatic approximation

The Schrödinger equation for a neutron is given by

$$\hat{H}\psi(\mathbf{r}, t) = i\hbar\partial\psi(\mathbf{r}, t)/\partial t, \quad (\text{A1})$$

where the Hamiltonian

$$\hat{H} = \hat{K} + \hat{V} = -\frac{\hbar^2\hat{\Delta}}{2m} + mgz + V_0\theta[-z + \xi(\mathbf{r}_{\parallel}, t)] \quad (\text{A2})$$

contains the neutron kinetic energy $\hat{K} = -\hbar^2\hat{\Delta}/2m$ and the potential energy $\hat{V} = mgz + V_0\theta[-z + \xi(\mathbf{r}_{\parallel}, t)]$. The latter contains the effects of the Earth's gravitational field and the potential wall due to the liquid helium, as shown in Fig. 1. The difference from Eq. (4) is that the liquid helium has now a time- and space-periodic boundary $\xi(\mathbf{r}_{\parallel}, t)$ given by Eq. (37). The difference between Eq. (A2) and Eq. (4) from Ref. [28] is that the surface has now a periodic spatial dependence.

The adiabatic adjustment of the neutron wave function to the new surface profile means that the neutron wave function, in first approximation, adiabatically shifts in z -direction by the length $\xi(\mathbf{r}_{\parallel}, t)$: $\psi(\mathbf{r}, t) \rightarrow \tilde{\psi}(\mathbf{r} + \xi(\mathbf{r}_{\parallel}, t)\hat{\mathbf{z}}, t)$, where $\hat{\mathbf{z}}$ is the unitary vector in z -direction. This shift can be written via the translation (z -shift) operator

$$\hat{T}_z(\xi) = \exp[\xi(\mathbf{r}_{\parallel}, t)\partial/\partial z] = \exp[i\xi(\mathbf{r}_{\parallel}, t)p_z/\hbar].$$

Its action on the wave function is

$$\hat{T}_z(\xi)\psi_{\perp}(z) = \psi_{\perp}(z + \xi).$$

We also define a new wave function

$$\tilde{\psi}(\mathbf{r} + \xi\hat{\mathbf{z}}, t) = \psi(\mathbf{r}, t) = \hat{T}_z(\xi)\tilde{\psi}(\mathbf{r}, t),$$

which after substitution into Eq. (A1) gives a new Schrödinger equation for $\tilde{\psi}(\mathbf{r}, t)$:

$$\hat{H}\hat{T}_z(\xi)\tilde{\psi}(\mathbf{r}, t) = i\hbar\partial(\hat{T}_z(\xi)\tilde{\psi}(\mathbf{r}, t))/\partial t. \quad (\text{A3})$$

The action of the shift operator on the potential energy function $V(\mathbf{r})$ is given by

$$V(\mathbf{r})\hat{T}_z(\xi) = \hat{T}_z(\xi)V(\mathbf{r} - \xi(\mathbf{r}_{\parallel}, t)\hat{\mathbf{z}}), \quad (\text{A4})$$

while for the commutator with kinetic-energy operator $\hat{K} = -\hbar^2\hat{\Delta}/2m$ we have

$$\begin{aligned} \hat{K}\hat{T}_z(\xi) - \hat{T}_z(\xi)\hat{K} &= -\frac{\hbar^2}{m}\left(\nabla^2 e^{\xi(\mathbf{r}_{\parallel}, t)\partial/\partial z} - e^{\xi(\mathbf{r}_{\parallel}, t)\partial/\partial z}\nabla^2\right) \\ &= \frac{2\hat{p}_{\parallel}\hat{p}_q + \hat{p}_q^2}{2m}\xi(\mathbf{r}_{\parallel}, t)\frac{\partial}{\partial z} = \frac{(\hat{p}_{\parallel} + \hat{p}_q)^2 - \hat{p}_{\parallel}^2}{2m}\xi(\mathbf{r}_{\parallel}, t)\frac{\partial}{\partial z}, \end{aligned} \quad (\text{A5})$$

where $\hat{p}_{\parallel} = -i\hbar\nabla_{\parallel}$ and $\hat{p}_q = \hbar q$ are the neutron and the ripplon momentum operators along the surface, respectively. The time-dependence of $\xi(\mathbf{r}_{\parallel}, t)$ also gives an additional term on the r.h.s. of Eq. (A3):

$$\begin{aligned} i\hbar\frac{\partial}{\partial t}\left(\hat{T}_z\tilde{\psi}(\mathbf{r}, t)\right) &= i\hbar\frac{\hat{T}_z\partial\tilde{\psi}(\mathbf{r}, t)}{\partial t} + i\hbar\frac{\partial\hat{T}_z}{\partial t}\tilde{\psi}(\mathbf{r}, t) \\ &= i\hbar\frac{\hat{T}_z\partial\tilde{\psi}(\mathbf{r}, t)}{\partial t} + \hbar\omega_q\xi(\mathbf{r}_{\parallel}, t)\frac{\partial}{\partial z}\hat{T}_z\tilde{\psi}(\mathbf{r}, t). \end{aligned} \quad (\text{A6})$$

Combining Eqs. (A3) and (A6) we obtain a new Schrödinger equation,

$$\hat{T}_z\left\{\hat{H}_0 + \hat{H}_{\text{int}} - i\hbar\partial/\partial t\right\}\tilde{\psi}(\mathbf{r}, t) = 0, \quad (\text{A7})$$

where \hat{H}_0 is given by Eq. (4) and the interaction term is given by

$$\hat{H}_{\text{int}} = \xi(\mathbf{r}_{\parallel}, t)\left\{\left[\frac{2\hat{p}_{\parallel}\hat{p}_q + \hat{p}_q^2}{2m} - \hbar\omega_q\right]\frac{\partial}{\partial z} + mg\right\}. \quad (\text{A8})$$

Appendix B: Crossover between adiabatic and diabatic limits in classical physics

For a classical particle above the surface in the limit $V_0 \rightarrow \infty$ the crossover between diabatic and adiabatic limits occurs when the maximal acceleration of the helium surface $\partial^2\xi_q/\partial t^2 = \omega_q^2\xi_q$, due to its oscillatory motion, becomes equal to the free fall acceleration g ,

$$\omega_{qc}^2\xi_q = g. \quad (\text{B1})$$

The classical amplitude ξ_q of the surface oscillations with wave vector \mathbf{q} differs from ξ_{0q} in Eq. (41) by the square

root of the Bose distribution function N_q given by Eq. (56):[77]

$$\xi_q = \sqrt{N_q \xi_{0q}} \approx \xi_{0q} \sqrt{k_B T / \hbar \omega_q}. \quad (\text{B2})$$

In addition, ξ_{0q} in Eq. (41) depends on the surface S , which must be defined. In the formulas for the neutron scattering rate by ripples this surface-dependence is unphysical and does not occur explicitly, because the S -dependence of the ripplon amplitude in Eq. (41) is compensated by the S -dependence of the ripplon density of states (see below). Similarly, the total mean square amplitude of thermal surface oscillations at any point r_{\parallel} is given by the sum over all \mathbf{q} -vectors,

$$\langle \xi^2(r_{\parallel}) \rangle = \sum_{\mathbf{q}} \xi_{\mathbf{q}}^2 = \int N_q \xi_{0q}^2 \frac{S d^2 \mathbf{q}}{(2\pi)^2},$$

and the surface area S drops out. More generally, if we are interested in the surface waves with the wave number q in some interval $\Delta q_x \Delta q_y$, then we sum all ripplon modes in the phase volume $S \Delta q_x \Delta q_y$, and the surface area S again drops out from the total $\langle \xi^2 \rangle$. In the estimate (B1) for the diabatic-adiabatic crossover the surface S is defined by the area S_n of the neutron wave function along the surface, which corresponds to the momentum smearing $\Delta q_x \Delta q_y \sim S_n^{-1}$.

For a lower estimate of ω_{qc} , leading to an upper estimate of the ripplon scattering rate, we take the minimal possible S given by the square of the wave length: $S_{\min} \approx (2\pi/q)^2$. Then, substituting it to Eq. (41), we have

$$\xi_{0q}^{\max} \approx \left(\frac{\hbar q^2}{8\pi^2 \sqrt{\rho \alpha q}} \right)^{1/2} = \frac{q^{3/4}}{2\pi} \left(\frac{\hbar/2}{\sqrt{\rho \alpha}} \right)^{1/2}. \quad (\text{B3})$$

For $q = 1 \mu\text{m}^{-1} = 10^4 \text{ cm}^{-1}$ this formula gives $\xi_{0q}^{\max} \approx 7 \times 10^{-5} \text{ nm}$, which is much less than q^{-1} . The corresponding

$$\xi_q^{\max} \approx \xi_{0q}^{\max} \sqrt{\frac{k_B T}{\hbar \omega_q}} = \frac{1}{2\pi} \left(\frac{k_B T}{2\alpha} \right)^{1/2} \approx 0.02 \text{ nm} \sqrt{T [\text{K}]} \quad (\text{B4})$$

is also much less than q^{-1} , and we can apply the usual surface wave description. Substituting $S_{\min} \approx (2\pi/q)^2$ to Eqs. (41), (B1) and (56) gives

$$g = \omega_{qc}^{3/2} \left(\frac{k_B T q^{3/2}}{2(2\pi)^2 \sqrt{\rho \alpha}} \right)^{1/2},$$

which, using Eq. (40), gives the lowest estimate for the crossover frequency

$$\omega_{qc} = \sqrt{2\pi g \sqrt{\frac{2\alpha}{k_B T}}} \approx \frac{6.6 \times 10^5 \text{ s}^{-1}}{(T [\text{K}])^{1/4}}. \quad (\text{B5})$$

This frequency corresponds to the neutron energy (at $T = 1 \text{ K}$) $\hbar \omega_{qc} \approx 7 \times 10^{-22} \text{ erg} \approx 0.44 \text{ neV} > E_0$ and to

$$q_c = 0.56 \mu\text{m}^{-1} > \varkappa. \quad (\text{B6})$$

Hence, in the diabatic limit $q > q_c$, and we can always use the ripplon dispersion given by Eq. (40).

Another condition of the classical adiabatic limit is that the curvature of the surface $\nabla^2 \xi = q^2 \xi_q^{\max}$ is less than the curvature of the neutron trajectory due to the parabolic free-fall motion $\partial^2 z / \partial r_{\parallel}^2 = g/v_{\parallel}^2$, where v_{\parallel} is the neutron velocity along the surface. Taking a UCN kinetic energy of $K_{\parallel} = 100 \text{ neV}$, corresponding to $v_{\parallel}^2 = 2K_{\parallel}/m = 19 \text{ m}^2/\text{s}^2$, we can check that the condition $q^2 \xi_q^{\max} < g/v_{\parallel}^2$ is fulfilled at $q = q_c = 0.56 \mu\text{m}^{-1}$. Hence, the condition $\omega_q < \omega_{qc}$ given by Eq. (B5) ensures the classical adiabatic limit.

Appendix C: Calculations for the neutron scattering rate due to ripples

In this section we evaluate the integral in Eq. (59) or (60), which gives the neutron scattering rate by ripples. The integration over p_q and n in Eqs. (59) can be separated into several regions, given by different limits of the ratio p_q/p_{\parallel} and of the difference $\Delta E_n - V_0$. For $\Delta E_n < V_0$ the final neutron vertical state belongs to a discrete energy spectrum, approximately given by Eq. (13). For $\Delta E_n > V_0$ the final neutron vertical state belongs to the continuous energy spectrum and can approximately be taken as a plane wave.

In the region $p_q \gg p_{\parallel}$ the initial neutron kinetic energy is negligible and, for the majority of the scattering events, the change of the neutron out-of-plane kinetic energy $\Delta E_n > V_0$. The integral in Eq. (59) is evaluated in this limit in Appendix C1 below.

In the region of small ripplon momentum, $p_q \lesssim p_{\parallel}$, studied in Appendix C2, the angle ϕ between the initial neutron and ripplon momenta is important for the out-of-plane energy transfer ΔE_n , and the scattering rate depends on the initial neutron momentum p_{\parallel} . Depending on the sign of the difference $\Delta E_n - V_0$, this region is split into two. For $\Delta E_n < V_0$ the final neutron state belongs to the discrete spectrum and is described by the formulas in Sec. II. For $\Delta E_n > V_0$ the final vertical neutron state belongs to the continuous spectrum and can be approximated by Eqs. (C2) and (C3).

1. Absorption of thermal (high-energy) ripples

In this subsection we consider the region of large momenta $p_q \gg p_{\parallel} = \sqrt{2Km}$ contributing to the integral in Eq. (59). Let us assume the in-plane kinetic energy K of ultra-cold neutrons being less than $K_* = 100 \text{ neV}$, which corresponds to a maximal initial neutron wave number $q_* = p_{\parallel}^*/\hbar = 7 \times 10^5 \text{ cm}^{-1} = 0.07 \text{ nm}^{-1}$ and to a maximal neutron velocity $v_{\parallel}^* = \sqrt{2K/m} = 4.4 \text{ m/s}$. For $q = q_*$ the ripplon energy, according to Eq. (40), is given

by

$$\hbar\omega_{q*} \equiv \hbar\omega_q(\hbar q = p_{\parallel*}) \approx 600 \text{ neV} \approx 7 \text{ mK} \gg V_0, K_*, \quad (\text{C1})$$

and the ripplon velocity is $v_{q*} = 3\omega_{q*}/2q_* = 20 \text{ m/s}$ [78]. If a ripplon with such a high energy is absorbed, the final out-of-plane neutron energy $E_n \sim \hbar\omega_q$ is much higher than the potential barrier $V_0 = 18.5 \text{ neV}$. It is then reasonable to take the final out-of-plane neutron wave function as a plane wave,

$$\psi_{\perp n}(z) \approx \exp(ip'_z z / \hbar) / \sqrt{L_z}. \quad (\text{C2})$$

Accordingly, the neutron out-of-plane energy can be approximated by the free-particle quadratic dispersion

$$E_n \approx p_z'^2 / 2m, \quad (\text{C3})$$

where p'_z is the component of the final neutron momentum perpendicular to the surface. The sum over out-of-plane neutron wave number n in Eq. (59) then becomes an integral over p'_z :

$$\sum_n \rightarrow \int \rho_n(p'_z) dp'_z, \quad (\text{C4})$$

where the one-dimensional neutron density of states is given by [79]

$$\rho_n(p'_z) \approx L_z / 2\pi\hbar. \quad (\text{C5})$$

For scattering by thermal ripples with $q > q_*$ the initial neutron energy $K \approx p_{\parallel}^2 / 2m$ and the momentum $p_{\parallel} < p_q$ can be neglected. Eqs. (57) and (58) then simplify to

$$\varepsilon \approx \hbar\omega_q; \quad \varepsilon' \approx (p_q^2 + p_z'^2) / 2m. \quad (\text{C6})$$

Using Eq. (39), we rewrite Eq. (59) as (the lower index ">" means large ripplon energy):

$$\begin{aligned} w_{>} &= \int_{\hbar q_*}^{\infty} \frac{\hbar |\psi_{\perp 0}(0) V_0|^2}{2\sqrt{\rho\alpha}q} \frac{N_q p_q dp_q}{2\pi\hbar^2} \\ &\times \int_0^{\infty} \frac{dp'_z}{\hbar^2} \delta\left(\hbar\omega_q - \frac{p_q^2 + p_z'^2}{2m}\right) \\ &= \int_{q_*}^{\infty} \frac{|\psi_{\perp 0}(0) V_0|^2}{2\pi\hbar\sqrt{\rho\alpha}} \frac{mN_q\sqrt{q}dq}{\sqrt{2m\hbar\omega_q - \hbar^2q^2}}. \end{aligned} \quad (\text{C7})$$

The square root in the denominator is real at $2m\hbar\omega_q = 2m\hbar\sqrt{\alpha/\rho}q^{3/2} > \hbar^2q^2$, which gives $q < 4q_0 \equiv (2m/\hbar)^2\alpha/\rho \approx 2.5 \text{ nm}^{-1}$ and corresponds to the ripplon energy $\hbar\omega_q < \hbar\omega_{q\text{max}} \approx \hbar(2m/\hbar)^3(\alpha/\rho)^2 = 2 \times 10^{-16} \text{ erg} = 1.25 \times 10^{-4} \text{ eV} \approx k_B \times 1.5 \text{ K} \gtrsim k_B T$. Above this energy the simple absorption of a ripplon by a UCN in a surface state is impossible because of the conservation laws for energy and momentum. Substituting Eqs.

(40) and (56) to Eq. (C7), and introducing the dimensionless variable $\zeta \equiv \hbar\omega_q/k_B T = \hbar\sqrt{\alpha/\rho}q^{3/2}/k_B T$, for which $q = \left(\zeta k_B T \sqrt{\rho/\alpha}/\hbar\right)^{2/3}$, we obtain

$$w_{>} = \frac{|\psi_{\perp 0}(0) V_0|^2 \sqrt{mk_B T}}{3\pi\hbar^2\alpha\sqrt{2}} \int_{\zeta_{\min}}^{\zeta_{\max}} \frac{\zeta^{-1/2} d\zeta (e^\zeta - 1)^{-1}}{\sqrt{1 - (\zeta/\zeta_{\max})^{1/3}}}, \quad (\text{C8})$$

where $\zeta_{\min} = \hbar\omega_{q*}/k_B T$ is given by Eq. (C1) and $\zeta_{\max} = \hbar\omega_{q\text{max}}/k_B T = (2m)^3(\alpha/\hbar\rho)^2/k_B T \sim 1$. The integration in Eq. (C8) diverges as $\zeta_{\min}^{-1/2}$ at the lower limit, and the main part of the integral comes from this divergence:

$$w_{>} \approx \frac{|\psi_{\perp 0}(0) V_0|^2 \sqrt{mk_B T}}{3\pi\hbar^2\alpha\sqrt{2}\sqrt{\zeta_{\min}}}. \quad (\text{C9})$$

Substituting the cutoff $\zeta_{\min} = \hbar\omega_{q*}/k_B T$ given by Eq. (C1) and other numerical values to Eq. (C9), we obtain the contribution to the neutron scattering rate from the high-energy ripples with $\hbar q > p_{\parallel*}$:

$$w_{>} \approx 1.7 \times 10^{-6} \text{ s}^{-1} \times T [\text{K}]. \quad (\text{C10})$$

At smaller ripplon energy, i.e. at $\hbar q < p_{\parallel*}$, the integral in Eq. (59) must be estimated without the approximation in Eqs. (C2)-(C6). In the next subsection we show that Eq. (C9) overestimates the integral in Eq. (59) for $\hbar q < p_{\parallel}$, especially for $\hbar\omega_q \lesssim V_0$ where the infrared divergence disappears.

At $K_* \rightarrow 0$, when the cutoff given by $q_* = \hbar/p_{\parallel*}$ is too small, the infrared divergence in Eq. (C9) must be cut off at $\zeta_{\min} \approx V_0/k_B T$, because the approximation given by Eqs. (C2)-(C5) is not valid for lower ripplon energies, for which the neutron state after the absorption still belongs to the discrete spectrum along the z -axis. A rough estimate of the absorption rate of high-energy ripples with $\hbar\omega_q > V_0$ can be obtained for small initial neutron energies $K < V_0$ by substituting $\zeta_{\min} \approx V_0/k_B T$ to Eq. (C9):

$$w_{>}^{\text{up}} \approx w_{>}(\zeta_{\min} \approx V_0/k_B T) \approx 10^{-5} \text{ s}^{-1} \times T [\text{K}]. \quad (\text{C11})$$

This estimate gives a neutron mean scattering time $1/w_{>}^{\text{up}} \approx 27 \text{ hours}$, which is much greater than the intrinsic neutron lifetime.

2. Upper estimate of the absorption rate of low-energy ripples

For $k_B T \gg \hbar\omega_q$ the ripplon population is given by $N_q \approx k_B T / \hbar\omega_q$. Substituting Eqs. (40) and (41) to Eq. (60) we obtain

$$w_{<} = \int_0^{p_{\text{max}}} \frac{k_B T dp_q^2}{4\pi\hbar\alpha p_q^2} \sum_n \frac{|\psi_{\perp 0}(0) \psi_{\perp n}^*(0) V_0|^2}{\sqrt{a^2 - (b - E_n)^2}}. \quad (\text{C12})$$

a. *Transitions to a continuous neutron spectrum*

In this subsection we consider the case of final neutron energies $E_n > V_0$ above the potential barrier and thus belonging to a continuous spectrum. We may then apply the approximation given by Eqs. (C2)-(C5) and rewrite Eq. (C12) as

$$w_{<} \approx \int_{p_{\min}}^{p_{\max}} \frac{k_B T dp_q^2}{4\pi\hbar\alpha p_q^2} \frac{|\psi_{\perp 0}(0) V_0|^2}{2\pi\hbar} I, \quad (\text{C13})$$

where the integral

$$I \equiv \int \frac{dp'_z}{\sqrt{a^2 - (b - p'_z/2m)^2}} = \int_{V_0}^{a+b} \frac{\sqrt{m/2E_n} dE_n}{\sqrt{a^2 - (b - E_n)^2}}. \quad (\text{C14})$$

For $b > a$ we may give an upper estimate of this integral:

$$I < I_{\max} = \frac{\sqrt{m}}{\sqrt{2V_0}} \int_{b-a}^{b+a} \frac{dE_n}{\sqrt{a^2 - (b - E_n)^2}} = \frac{\pi\sqrt{m}}{\sqrt{2V_0}}. \quad (\text{C15})$$

The corresponding upper estimate of Eq. (C13) is

$$w_{<}^{\text{up}} \approx \frac{k_B T |\psi_{\perp 0}(0) V_0|^2 \sqrt{m}}{4\pi\hbar^2 \alpha \sqrt{2V_0}} \ln \left(\frac{p_{\max}}{p_{\min}} \right). \quad (\text{C16})$$

The interval of integration $V_0 \leq E_n \leq b + a$ in Eq. (C14) is nonzero for $b + a \approx \hbar\omega_q + p_{\parallel} p_q / m > V_0$, which for $p_{\parallel}^2 / 2m = 100$ neV corresponds to $q > q_{\min} \equiv p_{\min} / \hbar \approx 4 \times 10^4$ cm⁻¹. Substituting also $\psi_{\perp 0}(0) \approx 0.236$ cm^{-1/2} and $p_{\max} = p_{\parallel*}$ to Eq. (C16), we obtain

$$w_{<}^{\text{up}} \approx 7.3 \times 10^{-6} \ln(q_*/q_{\min}) \times T [\text{K}] \approx 2 \times 10^{-5} \times T [\text{K}]. \quad (\text{C17})$$

b. *Transitions to the discrete neutron levels*

In this subsection we consider the case of final neutron energies in the interval $0 < \Delta E_n \lesssim V_0$ below the potential barrier and approximately given by Eqs. (13) and (15). Since $V_0 \gg E_0$, the sum over n in Eq. (C12) still includes many terms and can be approximated by an integration over n for $n \gg 1$. Eqs. (13) and (15) give $E_n \approx mgz_0 (3\pi n/2)^{2/3}$, which can be rewritten as

$$n \approx \frac{2}{3\pi} \left(\frac{\Delta E_n}{mgz_0} \right)^{3/2} = \frac{2(\Delta E_n)^{3/2}}{3\pi g\hbar} \sqrt{\frac{2}{m}}$$

and gives

$$\frac{dn}{dE_n} = \frac{\sqrt{E_n}}{\pi g\hbar} \sqrt{\frac{2}{m}}. \quad (\text{C18})$$

We also use that $|\psi_{\perp n}^*(0)| \lesssim \psi_{\perp 0}(0)$, and for an upper estimate of Eq. (C12) we replace $|\psi_{\perp n}^*(0)|$ by $|\psi_{\perp 0}(0)|$

for $E_n < V_0$. Using Eq. (C18), we rewrite Eq. (C12) for $\Delta E_n < V_0$ as

$$w_{\ll} \approx \int_0^{p_{\max}} \frac{k_B T dp_q}{\pi\hbar^2 \alpha p_q} \frac{|\psi_{\perp 0}(0) V_0|^2}{\pi g \sqrt{2m}} \int_0^{V_0} \frac{\sqrt{E_n} dE_n}{\sqrt{a^2 - (b - E_n)^2}}. \quad (\text{C19})$$

This integral converges, with main contributions from $E_n \sim V_0$. The upper estimate w_{\ll}^{up} of this integral can be obtained by replacing $\sqrt{E_n}$ by $\sqrt{V_0}$ in the integrand and by extending the integration region from $(0, V_0)$ to $(a - b, a + b)$. This gives an integral over E_n similar to Eq. (C15):

$$\begin{aligned} w_{\ll}^{\text{up}} &= \int_{p_{\min}}^{p_{\max}} \frac{k_B T dp_q}{\pi\hbar^2 \alpha p_q} \frac{|\psi_{\perp 0}(0) V_0|^2 \sqrt{V_0}}{\pi g \sqrt{2m}} \\ &\quad \times \int_{b-a}^{b+a} \frac{dE_n}{\sqrt{a^2 - (b - E_n)^2}} \\ &= \frac{k_B T |\psi_{\perp 0}(0) V_0|^2 \sqrt{V_0}}{\pi\hbar^2 \alpha g \sqrt{2m}} \ln \left(\frac{p_{\max} V_0}{p_{\min} V_0} \right). \end{aligned} \quad (\text{C20})$$

Since $V_0 > E_n$ and the integrand in Eq. (C19) is real for $b - a < E_n < b + a$, the region of integration over E_n in Eq. (C19) is nonzero if $b - a \approx \hbar\omega_q - p_{\parallel} p_q / m < V_0$, which for $p_{\parallel}^2 / 2m = 100$ neV corresponds to $p_q < p_{\max} \approx \hbar q_{\max} V_0$ with $q_{\max} V_0 = 1.57 \times 10^5$ cm⁻¹. On the other hand, $\Delta E_n < b + a$ can reach V_0 if $b + a \approx \hbar\omega_q + p_{\parallel} p_q / m \geq V_0$. For $p_{\parallel}^2 / 2m = 100$ neV this gives $p_q > p_{\min} V_0 \approx \hbar q_{\min} V_0$ with $q_{\min} V_0 = 3.8 \times 10^4$ cm⁻¹. For $p_q < p_{\min} V_0$ the logarithmic divergence disappears. Hence, using Eq. (C20) we obtain an upper estimate of w_{\ll} :

$$w_{\ll}^{\text{up}} \approx 4 \times 10^{-5} \times T [\text{K}] \text{ s}^{-1}. \quad (\text{C21})$$

Appendix D: Scattering of neutrons by surfons

1. Matrix element

A surfon, being a ⁴He atom on the surface energy level [48, 49], interacts with a neutron via the potential given in Eq. (1). The matrix elements of neutron-He interaction in Eqs. (24),(29) assumes that the He wave function is a plane wave also along the z -axis, which is not the case for the surfons. Therefore, in this subsection we derive the neutron-surfon matrix element in the way similar to that in Sec. IIIA.

The surfon wave function is given by a product $\Psi = \Psi_{\perp}(z) \Psi_{\parallel}(\mathbf{r}_{\parallel})$. The parallel-to-surface surfon wave function is a plane wave: $\Psi_{\parallel}(\mathbf{r}_{\parallel}) = \exp(i\mathbf{P}_{\parallel} \mathbf{r}_{\parallel} / \hbar)$. The perpendicular-to-surface surfon wave function $\Psi_{\perp}(z)$ was analyzed in Refs. [49–51] and shown to be localized above the surface on a height ~ 0.4 nm $\ll z_0$ [81]. Hence, for our calculation we may take $\Psi_{\perp}^2(z) \approx \delta(z)$. The initial and final surfon wave functions differ only by the initial and final

momentum, \mathbf{P}_{\parallel} and \mathbf{P}'_{\parallel} , respectively. On the other hand, the neutron out-of-plane wave function strongly changes due to the scattering on a surfon, and for the majority of events it gets transferred from the discrete to the continuous spectrum. Hence, the final neutron wave function is given by Eq. (23). The matrix element of the interaction potential (1) is given by

$$T_{\text{if}} = U \int d^3\mathbf{r} \psi_{\perp 0}(z) \psi_{\parallel}(\mathbf{r}_{\parallel}) \psi'(\mathbf{r}) \times \\ \int d^3\mathbf{R} \psi \Psi_{\perp}^2(z) \exp \left[\frac{i(\mathbf{P}_{\parallel} - \mathbf{P}'_{\parallel}) \cdot \mathbf{R}_{\parallel}}{\hbar} \right] \delta^{(3)}(\mathbf{r} - \mathbf{R}) \\ \approx U \psi_{\perp 0}(0) (2\pi\hbar)^2 \delta^{(2)}(\Delta\mathbf{P}_{\text{tot}\parallel}) / \sqrt{SV}, \quad (\text{D1})$$

where $\Delta\mathbf{P}_{\text{tot}} \approx \mathbf{P} - \mathbf{P}' - \mathbf{p}'$ is the change of total momentum and \mathbf{R} is the surfon coordinate. Below we need only the square of the absolute value of the matrix element T_{if} . The square of the δ -function in $|T_{\text{if}}|^2$ should be treated using Eq. (28). Then instead of Eq. (29) we obtain

$$|T_{\text{if}}|^2 = U^2 \psi_{\perp 0}^2(0) (2\pi\hbar)^2 \delta^{(2)}(\Delta\mathbf{P}_{\text{tot}\parallel}) / V. \quad (\text{D2})$$

2. Scattering rate

The scattering rate of a neutron by a surfon with initial momentum \mathbf{P}_{\parallel} is given by the square of the matrix element (29) integrated over the final momenta \mathbf{p}' and \mathbf{P}'_{\parallel} of the neutron and surfon, respectively (Fermi's golden rule [38]),

$$w_{\mathbf{p}} = \frac{2\pi}{\hbar} \int \frac{d^2\mathbf{P}'_{\parallel}}{(2\pi\hbar)^2} \int \frac{V d^3\mathbf{p}'}{(2\pi\hbar)^3} |T_{\text{if}}|^2 \delta(\varepsilon - \varepsilon'). \quad (\text{D3})$$

Here $\varepsilon \approx P_{\parallel}^2/2M$ and $\varepsilon' = P_{\parallel}^2/2M + p'^2/2m$ are the initial and final total energies of surfon + neutron, respectively. We now substitute them and Eq. (D2) to Eq. (D3). The integration over \mathbf{p}'_{\parallel} cancels $\delta^{(2)}(\Delta\mathbf{P}_{\text{tot}\parallel})$ in the matrix element in Eq. (D2), where $\Delta\mathbf{P}_{\text{tot}\parallel} \approx \mathbf{P}_{\parallel} - \mathbf{P}'_{\parallel} - \mathbf{p}'$:

$$w_{\mathbf{p}} = \frac{U^2 |\psi_{\perp 0}^2(0)|}{\hbar^3} \int \frac{P_{\parallel} dP'_{\parallel}}{2\pi} \frac{dp'_{\perp}}{2\pi\hbar} \int d\phi \delta(\varepsilon - \varepsilon'). \quad (\text{D4})$$

Substituting ε and ε' , and integrating over the angle ϕ between \mathbf{P}_{\parallel} and \mathbf{P}'_{\parallel} , we obtain

$$w_{\mathbf{p}} = \frac{U^2}{\hbar^3} |\psi_{\perp 0}^2(0)| \int \frac{P'_{\parallel} dP'_{\parallel}}{2\pi} \frac{dp'_{\perp}}{2\pi\hbar} \times \\ \left[\left(\frac{P'_{\parallel} P_{\parallel}}{m} \right)^2 - \left(\frac{P_{\parallel}^2}{2M} - \frac{P'_{\parallel}{}^2}{2M} - \frac{P_{\parallel}^2 + P'_{\parallel}{}^2 + p'_{\perp}{}^2}{2m} \right)^2 \right]^{-1/2}. \quad (\text{D5})$$

Now we use $M = 4m$ to simplify this expression:

$$w_{\mathbf{p}} = \int \frac{(U^2 m |\psi_{\perp 0}^2(0)| / 4\pi^2 \hbar^4) P'_{\parallel} dP'_{\parallel} dp'_{\perp}}{\sqrt{P'_{\parallel} P_{\parallel}^2 - [P_{\parallel}^2/8 - P'_{\parallel}{}^2/8 - (P_{\parallel}^2 + P'_{\parallel}{}^2 + p'_{\perp}{}^2)/2]^2}}.$$

Introducing new dimensionless integration variables $x_p \equiv P'_{\parallel}{}^2/P_{\parallel}^2$ and $y_p \equiv p'_{\perp}/P_{\parallel}$, we rewrite this as

$$w_{\mathbf{p}} = \frac{U^2 m P_{\parallel}}{\pi^2 \hbar^4} \int \frac{|\psi_{\perp 0}^2(0)| dx_p dy_p}{\sqrt{64x_p - (3 + 5x_p + 4y_p^2)^2}}. \quad (\text{D6})$$

This may be further transformed to

$$w_{\mathbf{p}} = \frac{U^2 m P_{\parallel}}{\pi^2 \hbar^4} \int \frac{|\psi_{\perp 0}^2(0)| dx_p dy_p}{\sqrt{(y_p^2 - b_1)(b_2 - y_p^2)}} \quad (\text{D7})$$

$$= \frac{U^2 m P_{\parallel}}{\pi^2 \hbar^4} \int \frac{|\psi_{\perp 0}^2(0)| dx_p dy_p}{5\sqrt{(x_p - a_1)(a_2 - x_p)}}, \quad (\text{D8})$$

where the solutions of square-root equations are

$$b_{1,2} = \frac{-3 \mp 8\sqrt{x_p} - 5x_p}{4}, \quad (\text{D9})$$

and

$$a_{1,2} = \frac{17 \mp 8\sqrt{1 - 20y_p^2} - 20y_p^2}{25}. \quad (\text{D10})$$

The integral over x_p in Eq. (D8) gives π for any $a_2 > a_1$, however, the integrand is real only for some values of y_p^2 . The maximum value of b_2 in Eq. (D9) is $b_2^{\text{max}} = 0.2$ at $x_p = 16/25$. Since $0 < y_p^2 < b_2^{\text{max}}$, for an upper estimate of the integral in Eq. (D6) we may take

$$w_{\mathbf{p}}^{\text{up}} = \frac{U^2 m P_{\parallel}}{\pi^2 \hbar^4} \int \frac{|\psi_{\perp 0}^2(0)| dx_p 2\sqrt{b_2^{\text{max}}}}{5\sqrt{(x_p - a_1)(a_2 - x_p)}} \\ = \frac{U^2 m P_{\parallel}}{\pi^2 \hbar^4} |\psi_{\perp 0}^2(0)| \frac{2\pi\sqrt{0.2}}{5}. \quad (\text{D11})$$

The total scattering rate is given by the integral over all initial surfon states with corresponding populations:

$$\frac{w_{\text{sur}}^{\text{up}}}{|\psi_{\perp 0}^2(0)|} = \int \frac{d^2\mathbf{P}_{\parallel}}{(2\pi\hbar)^2} w_{\mathbf{p}}^{\text{up}} \exp\left(\frac{-\Delta_{s0} - \mathbf{P}_{\parallel}^2/2M}{k_{\text{B}}T}\right).$$

Substituting Eq. (D11) and performing the integration we obtain

$$\frac{w_{\text{sur}}^{\text{up}}}{|\psi_{\perp 0}^2(0)|} = \frac{U^2 m \sqrt{1.6\pi}}{20\pi^2 \hbar^6} \exp\left(\frac{-\Delta_{s0}}{k_{\text{B}}T}\right) (M k_{\text{B}}T)^{3/2}.$$

Substituting U from Eq. (1) we obtain the scattering rate given by Eq. (70), which is negligibly small.

-
- [1] D. Dubbers and M. G. Schmidt, Rev. Mod. Phys. **83**, 1111 (2011).
- [2] M. J. Ramsey-Musolf and S. Su, Phys. Rept. **456**, 1 (2008).
- [3] H. Abele, Prog. Nucl. Phys. **60**, 1 (2008).
- [4] R. Golub, D. J. Richardson, S. K. Lamoreaux, *Ultra-Cold Neutrons* (Adam Hilger, Bristol 1991).
- [5] V. K. Ignatovich, *The Physics of Ultracold Neutrons* (Oxford Science Publications, Clarendon Press, Oxford, 1990).
- [6] E. M. Purcell, and N. F. Ramsey, Phys. Rev. **78**, 807 (1950).
- [7] M. Pospelov and A. Ritz, Annals Phys. **318**, 119 (2005).
- [8] C. A. Baker et al., Phys. Rev. Lett. **97**, 131801 (2006).
- [9] A. P. Serebrov, E. A. Kolomenskiy, A. N. Pirozhkov et al., JETP Lett. **99**, 4 (2014) [Pis'ma v ZhETF **99**, 7 (2014)].
- [10] A. Coc, N. J. Nunes, K. A. Olive et al., Phys. Rev. D **76**, 023511 (2007).
- [11] R. E. Lopez and M. S. Turner, Phys. Rev. D **59**, 103502 (1999).
- [12] V. I. Luschikov, A. I. Frank, JETP Lett. **28**, 559 (1978).
- [13] V. V. Nesvizhevsky, H. G. Börner, A. K. Petukhov, H. Abele, S. Baessler, F. J. Ruess, T. Stöferle, A. Westphal, A. M. Gagarski, G. A. Petrov, and A. V. Strelkov, Nature (London) **415**, 297 (2002).
- [14] V. V. Nesvizhevsky, A. K. Petukhov, H. G. Börner, T. A. Baranova, A. M. Gagarski, G. A. Petrov, K. V. Protasov, A. Y. Voronin, S. Baessler, H. Abele, A. Westphal, and L. Lucovac, Eur. Phys. J. C **40**, 479 (2005).
- [15] A. Westphal, H. Abele, S. Baessler, V. Nesvizhevsky, K. Protasov, and A. Voronin, Eur. Phys. J. C **51**, 367 (2007).
- [16] N. Arkani-Hamed, S. Dimopoulos, G. Dvali, Phys. Rev. D **59**, 086004 (1999).
- [17] I. Antoniadis, Lect. Notes Phys. **631**, 337 (2003).
- [18] P. Brax, G. Pignol, Phys. Rev. Lett. **107**, 111301 (2011).
- [19] T. Jenke, G. Cronenberg, J. Burgdörfer, L. A. Chizhova, P. Geltenbort, A. N. Ivanov, T. Lauer, T. Lins, S. Rotter, H. Saul, U. Schmidt, and H. Abele, Phys. Rev. Lett. **112**, 151105 (2014).
- [20] T. Jenke, P. Geltenbort, H. Lemmel, H. Abele, Nature Phys. **7**, 468(2011).
- [21] P. Hamilton, M. Jaffe, P. Haslinger, Q. Simmons, H. Müller, J. Khoury, Science **349**, 849 (2015).
- [22] M. Kreuz, V. Nesvizhevsky, P. Schmidt-Wellenburg, T. Soldner et al., Nucl. Instr. Meth. A **611**, 326 (2009).
- [23] G. Pignol, S. Baessler, V. V. Nesvizhevsky et al., Adv. High Energy Phys. **2014**, 628125 (2014).
- [24] S. Baessler, V. V. Nesvizhevsky, K. V. Protasov, A. Y. Voronin, Phys. Rev. D **75**, 075006 (2007).
- [25] O. Zimmer, Phys. Lett. B **685**, 38 (2010).
- [26] A. P. Serebrov, O. Zimmer, P. Geltenbort et al., JETP Lett. **91**, 6 (2010).
- [27] S. Afach et al., Phys. Lett. B **745**, 58 (2015).
- [28] H. Abele, T. Jenke, H. Leeb, and J. Schmiedmayer, Phys. Rev. D **81**, 065019 (2010).
- [29] K. Durstberger-Rennhofer, T. Jenke, H. Abele, Phys. Rev. D **84**, 036004 (2011).
- [30] V. B. Shikin and Yu. P. Monarkha, *Two-Dimensional Charged Systems in Helium* (in Russian), Nauka, Moscow (1989).
- [31] V. S. Edel'man, Sov. Phys. - Uspehi **130**, 676 (1980).
- [32] Y. Monarkha, K. Kono, *Two-Dimensional Coulomb Liquids and Solids*, Springer Verlag, 2004.
- [33] G. Papageorgiou, P. Glasson, K. Harrabi, et al., Appl. Phys. Lett. **86**, 153106 (2005).
- [34] B. A. Nikolaenko, Yu. Z. Kovdrya, and S. P. Gladchenko, Journal of Low Temp. Phys. (Kharkov) **28**, 859 (2002).
- [35] A. M. Dyugaev, A. S. Rozhavskii, I. D. Vagner and P. Wyder, JETP Lett. **67**, 434 (1998).
- [36] P. M. Platzman, M. I. Dykman, Science **284**, 1967 (1999); M. I. Dykman, P. M. Platzman, and P. Seddighrad, Phys. Rev. B **67**, 155402 (2003).
- [37] Since the chemical potential of liquid helium $|\mu| \gg k_B T$, the Boltzmann distribution does not differ from the Bose-Einstein distribution.
- [38] L. D. Landau and E.M. Lifshitz, Course of Theoretical Physics, Vol. 3: Quantum Mechanics, 3rd ed., Pergamon Press, Oxford, 1977.
- [39] L. D. Landau and E.M. Lifshitz, Course of Theoretical Physics, Vol. 6: Hydrodynamics, 3rd ed., Pergamon Press, Oxford.
- [40] Yu. P. Monarkha and V. B. Shikin, "Low-dimensional electronic systems on a liquid helium surface (Review)", Sov. J. Low Temp. Phys. **8**, 279 (1982).
- [41] Eq. (39) can be obtained[30] by equating the energy of a classical surface wave with the wave number q and amplitude ξ_{0q} on the area S , given in §12,25,62 of Ref. [39], to the energy $\hbar\omega_q$ of one ripplon.
- [42] E. Eidelstein, D. Goberman, and A. Schiller, Phys. Rev. B **87**, 075319 (2013).
- [43] R. Citro, E. Orignac, and T. Giamarchi, Phys. Rev. B **72**, 024434 (2005).
- [44] Balazs Dora, Masudul Haque, and Gergely Zarand, Phys. Rev. Lett. **106**, 156406 (2011).
- [45] D. A. Ivanov and M. V. Feigel'man, ZhETF **114**, 640 (1998) [JETP, **87**(2), 349 (1998)].
- [46] Kazuki Koshino and Tetsuo Ogawa, Journal of the Korean Physical Society **34**, S21 (1999).
- [47] R. Golub, Phys. Lett. A **72**, 387 (1979).
- [48] A. M. Dyugaev, P. D. Grigoriev, JETP Lett. **78**, 466 (2003).
- [49] A. D. Grigoriev, P. D. Grigoriev, A. M. Dyugaev, J. Low Temp. Phys. **163**, 131 (2011).
- [50] A. D. Grigoriev, P. D. Grigoriev, A. M. Dyugaev, A. F. Krutov, Low Temp. Phys., **38** (11), 1005 (2012).
- [51] P. D. Grigoriev, A. M. Dyugaev, E. V. Lebedeva, JETP **106**, 316 (2008) [ZhETF **133**, 370 (2008)].
- [52] O. Zimmer, F.M. Piegsa, S.N. Ivanov, Phys. Rev. Lett. **107**, 134801 (2011).
- [53] F.M. Piegsa, M. Fertl, S.N. Ivanov et al., Phys. Rev. C **90**, 015501 (2014).
- [54] O. Zimmer, K. Baumann, M. Fertl et al., Phys. Rev. Lett. **99**, 104801 (2007).
- [55] O. Zimmer, P. Schmidt-Wellenburg, M. Fertl et al., Eur. Phys. J. C **67**, 589 (2010).
- [56] R. Golub and J. M. Pendlebury, Phys. Lett. **53A**, 133 (1975).
- [57] R. Golub, J. Pendlebury, Phys. Lett. A **82**, 337 (1977).
- [58] P. Ch. Bokun, Sov. J. Nucl. Phys. **40** (1), 180 (1984) [Yad. Fiz. **40**, 287 (1984)].
- [59] V. P. Alfimenkov, V. K. Ignatovich, L. P. Mezhov-Deglin, V. I. Morozov, A. V. Strelkov, M. I. Pulaja, Comm. Joint

- Inst. Nucl. Research, Dubna preprint P3-2009-197 (2009) [in Russian].
- [60] V. F. Ezhov, A. Z. Andreev, G. Ban et al., arXiv:1412.7434 (2014).
- [61] D. J. Salvat, E. R. Adamek, D. Barlow et al., Phys. Rev. C **89**, 052501 (2014).
- [62] K. Leung, S. Ivanov, F. Martin et al., Proceedings of the workshop “Next Generation Experiments to Measure the Neutron Lifetime”, Santa Fe, New Mexico, 9 – 10 November 2012, page 145. World Scientific (2014).
- [63] V. F. Ezhov, A. Z. Andreev, G. Ban et al., Nucl. Instr. Meth. A **611**, 167 (2009).
- [64] K. K. H. Leung, O. Zimmer, Nucl. Instr. Meth. A **611**, 181 (2009).
- [65] R. Picker, I. Altarev, J. Bröcker et al., J. Res. NIST **110**, 357 (2005).
- [66] P. R. Huffman, C. R. Brome, J. S. Butterworth et al., Nature **403**, 62 (2000).
- [67] O. Zimmer, J. Phys. G: Nucl. Part. Phys. **26**, 67 (2000).
- [68] F. E. Wietfeldt, G. L. Greene, Rev. Mod. Phys. **83**, 1173 (2011).
- [69] S. Paul, Nucl. Instr. Meth. A **611**, 157 (2009).
- [70] M. Daum, P. Fierlinger, B. Franke, P. Geltenbort et al., Phys. Lett. B **704**, 456 (2011).
- [71] T. Brenner, S. Chesnevskaya, P. Fierlinger et al., Phys. Lett. B **741**, 316 (2015).
- [72] O. Zimmer, R. Golub, Phys. Rev. C **92**, 015501 (2015).
- [73] K. P. Hickerson, B. W. Filippone, Nucl. Instr. Meth. A **721**, 60 (2013).
- [74] A. Steyerl, W. Drexel, S. S. Malik, E. Gutschiedl, Physica B **151**, 36 (1988).
- [75] Y. Arimoto, P. Geltenbort, S. Imajo, Y. Iwashita et al., Phys. Rev. A **86**, 023843 (2012).
- [76] C. Siemensen, D. Brose, L. Böhmer, P. Geltenbort, C. Plonka-Spehr, Nucl. Instr. Meth. A **778**, 26 (2015).
- [77] The thermally excited riplons are not coherent, therefore the population factor N_q increases the mean energy of the surface wave by N_q times, not the amplitude of thermal riplons, which is increased only by $\sqrt{N_q}$ times.
- [78] The typical thermal ripplon has even larger energy $\hbar\omega_q \sim k_B T \approx 0.5$ K, corresponding to the wave number $q \approx 1.2$ nm⁻¹ and the velocity $v_q \equiv \partial\omega_q/\partial q \approx 82$ m/s.
- [79] Eqs. (C2)-(C4) can also be applied for smaller E_n if $p'_z = p'_z(z)$ is understood as a quasi-classical coordinate-dependent momentum; then in Eq. (C3) one then should take its value at $z = 0$, and $\rho_n(p'_z)$ differs from Eq. (C5) and depends on the actual spectrum.
- [80] The integrand in Eq. (60) is real at $b - a \leq \Delta E_n \leq b + a$. The quantity $b > a$ at $p_{\parallel} < m\sqrt{\alpha q/\rho} - \hbar q/2$, which for $p_{\parallel}^2/2m = 100$ neV corresponds to $q > p_{\parallel}^2\rho/m^2\alpha \approx 8 \times 10^4$ cm⁻¹ and $\hbar\omega_q > 23$ neV.
- [81] According to Eq. (10) of Ref. [50], $\psi_{s\perp}(z) \approx 2\kappa_s^{3/2}(z - z_s)\exp[-\kappa_s(z - z_s)]$ with $\kappa_s \approx 8.7$ nm⁻¹ and $z_s \approx 0.175$ nm (see also Fig. 1 in Ref. [50]).